ELSEVIER

Polymer 41 (2000) 8983–9001

polymer

www.elsevier.nl/locate/polymer

Some "overlooked problems" in polymer crystallization

P.H. Geil*

Department of Materials Science and Engineering, University of Illinois, 1304 W. Green Street, Urbana, IL 61801, USA

Received 4 October 1999; received in revised form 7 December 1999; accepted 29 December 1999

Abstract

A number of observations of the morphology of crystalline polymers are described that, we believe, are not adequately explained in terms of current theory and modeling. These include evidence for primary nuclei of excessive thickness, linear variations in planar growth face directions with crystallization temperature, fold planes parallel (only) to the long axis of solution grown crystals, lamellar doubling in melt crystallized lamellae, discrepancies between small angle X-ray scattering (SAXS) and electron microscopy measurements of lamellar thickness and in the SAXS periodicities, and the effects of a molten free surface on the resulting morphology following crystallization.

Keywords: Polymer morphology; Lamellar doubling; Fold planes

1. Introduction

By the time this article is published it will be 44 years since I first saw Paul Till's electron micrographs and electron diffraction (ED) patterns (some of these micrographs were published in Ref. [1], being in press at the same time as Refs. [2,3]), taken with an RCA EMU 2, of (essentially)[1] linear polyethylene (LPE) while interviewing at the Polychemicals Department, DuPont Experimental Station. Having been enticed by the promise I could conduct research in the area of polymer morphology if accepting employment, I, and later my students, have since taken thousands of electron micrographs and diffraction patterns of LPE and other polymers, crystallized from solution, melt, liquid crystalline state and as-polymerized. Although one could and would hope that by now polymer crystallization would both be well understood and the knowledge practically applied, I suggest there are a number of fundamental observations that have not, to my knowledge, been considered in the various models and theories of polymer crystallization. In part, I suggest, this is because theory has been based primarily on observations of polyethylene crystallization. We discuss here some of these observations and resulting problems, based primarily on micrographs and small angle X-ray scattering (SAXS) data my students and I have taken. Four areas are considered, all with some overlap: primary nucleation, growth face lattice indices (lamella shape), lamellar doubling and the relationship between SAXS and transmission electron microscopy (TEM) shadow angle measurements of lamellar thickness, and free surface effects. Most of the observations were published more than 25 years ago, some in publications no longer readily available; these are supplemented by a few, more recent, relevant observations.

2. Experimental

Sample preparation conditions for all samples described here are given in the original publications; necessary descriptions will be given in the text or figure captions.

3. Observations

3.1. Primary nucleation

It is generally accepted that the homogeneous, primary nucleus of a folded chain lamella is close to twice the thickness of the secondary nuclei giving rise to the fold planes in the growing crystal [4] (also see Ref. [5] for a recent review with particular emphasis on crystallization from the melt of polyethylene). In solution grown, single lamella, single crystals the apparent primary nuclei have occasionally been observed as bumps in the centers of the crystals; an example is shown in Fig. 1. In this sample of

* Tel.: +1-217-333-0149; fax: +1-217-333-2736.
E-mail address: geil@uiuc.edu (P.H. Geil).

[1] Due to a composition of matter patent case being litigated while I was at DuPont, DuPont lawyers required the use of the term "essentially" linear polyethylene even for LPE having less than 1 branch/1000 C atoms.

0032-3861/00/$ - see front matter
PII: S0032-3861(00)00241-X

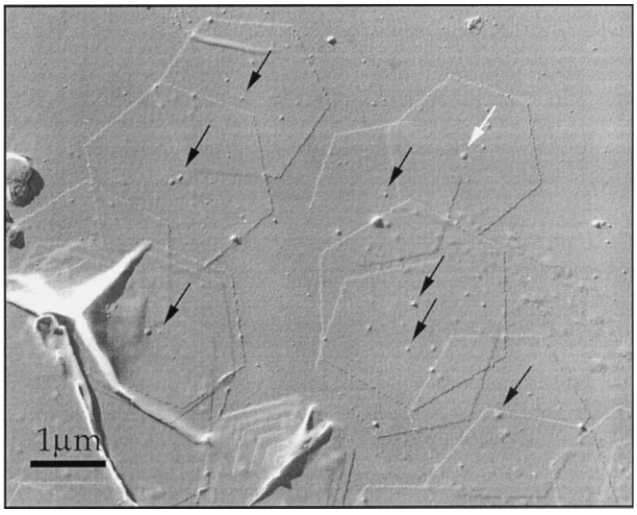

Fig. 1. Primary nuclei (arrows) in POM (ethylene oxide copolymer, $\bar{M}_n$ ca. 40,000, melting point depression 6°C, comonomer content not known) single crystals grown by slow cooling of a 0.5% solution in bromobenzene from 155°C. The white arrow indicates a primary nucleus that was thick enough to nucleate a second layer, probably when the temperature became low enough that a thin layer would be stable. Similar nuclei were also observed in the homopolymer [6].

polyoxymethylene–ethylene oxide copolymer crystallized from bromobenzene by cooling [6], the bumps vary somewhat in both diameter and height, but only in the case of the bump indicated by the white arrow is the thickness of the nucleus sufficient to give rise to the nucleation of more than one lamella. Because of the small lateral dimension of the upper lamellae we suggest it may have been nucleated following settling of the crystal on the substrate, the nucleus being forced through the crystal and residual low molecular weight polymer in the solution crystallizing out around the

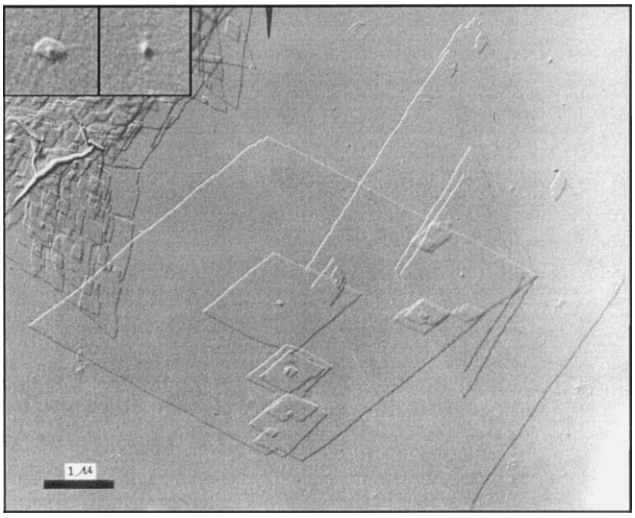

Fig. 2. Primary nuclei in BCMO ($\bar{M}_n$ ca. 300,000) crystallized from a 0.1% solution in xylene by ambient cooling. More than 80% of the crystals were similar in appearance to the crystal on the right, having an additional, half size lamella on each side of the larger central one. The apex angle is ca. 60° [7].

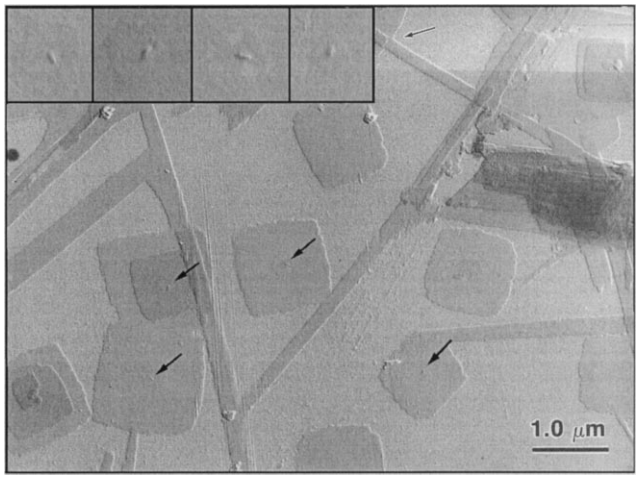

Fig. 3. Primary nuclei (insets and black arrows) in extended chain crystals of poly(*m*-oxybenzoate/2,6-naphthoate) (1/1) prepared by the CTFMP technique at 180°C for 5 h. The upper arrow indicates a region in which a nearly square crystal overlaps a lath-like crystal, suggesting the square crystals, at least, grew suspended in the monomer melt rather than on the substrate [10].

now projecting nucleus before and during solvent evaporation. Although these results thus agree with expectations, none of the other crystals shown in the same paper, of polyoxymethylene–ethylene oxide copolymers of differing composition, nor other polyoxymethylene homopolymers we have observed, have had similar "bumps".

In the preparation of poly(3,3-bis(chloromethyl)-oxacyclobutane) (BCMO) (Penton, a product of Hercules Co. Inc. $\bar{M}_n = 300,000$) shown in Fig. 2 [7] all crystals had a bump at their center and most had, in addition, two "extra" lamellae, one on the top surface and one underneath as shown by the curvature (rather than shear) of the largest lamella where it overlies the edge of the lamella that is underneath. These two "extra" lamellae were nearly always ca. 1/2 the lateral dimension of the central lamella; only occasionally, as in the crystal on the left in Fig. 2, is only a single "extra" lamella present, or as here, a second, small, "extra" lamella. These crystals were grown by dissolving the pellets supplied by Hercules in xylene at an elevated temperature followed by cooling. The "half-size" of the two "extra" lamellae was attributed to their being able to obtain polymer from the solution from only a hemisphere on the surface of the central lamella whereas the faster growing central lamella has a sphere of solution in contact with its growth face from which to "extract" polymer molecules for growth.

A possible explanation for the primary nuclei in this preparation being more than three times the thickness of the growth lamellae would be the presence of self-seeding [8], nuclei being retained from the pellets used for preparing the solution. This we doubt, since the pellets would have been quenched and thus would be expected to have low melting, thin lamellae, but cannot rule out based on the experimental data available. It is noted that some other (see Fig. 4 below), but not all, preparations of BCMO single crystals showed the thick nuclei and "extra" lamellae [7,9].

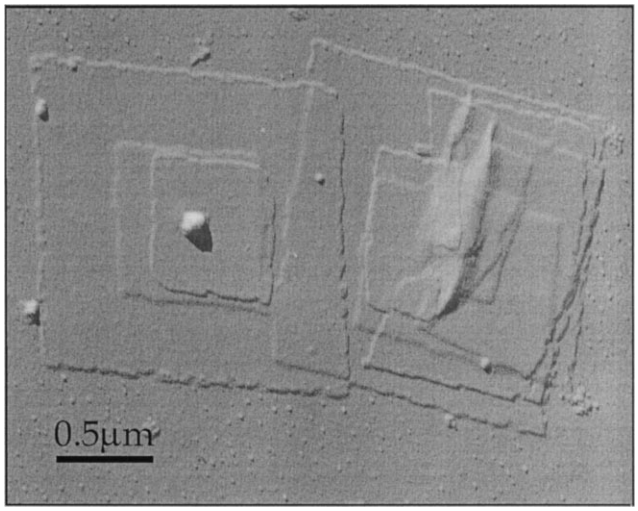

Fig. 4. Single crystals of BCMO crystallized isothermally from 0.05% solution in *n*-butyl acetate at 104°C, followed by annealing at 162°C after deposition on a slide. The initial crystals had a thin edge resulting from polymer addition during cooling; this is the only part that thickened during annealing. The apex angle is 84°. The central particle on the crystal on the left is an artifact hiding the primary nucleus [9].

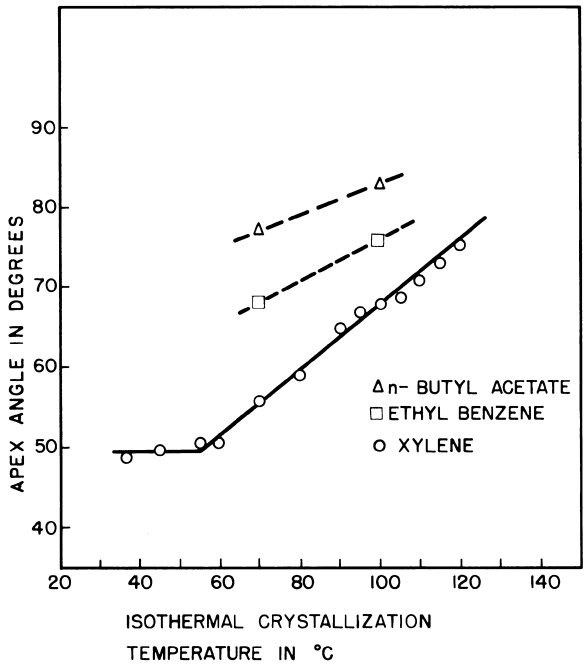

Fig. 5. Plot of apex angle vs. isothermal crystallization temperature for BCMO crystallized from several solvents. Reproduced from Ref. [7].

Thus one is left with the need for an explanation for the fold period of the primary nuclei being more than three times the fold period of the resulting crystals.

We have also apparently observed the primary nuclei in a sample [10] of a presumably random, liquid crystalline, copolymer, poly(*m*oxybenzoate-2,6-oxynaphthoate) (1/1), (P(*m*OBA/ONA) simultaneously polymerized and crystallized by our confined thin film melt polymerization technique (CTFMP) [11]. This polymer presumably polymerizes in the liquid crystalline state and transforms to the crystalline state, as shown by ED patterns, when the chains become long enough or during cooling. Two morphologies are seen (Fig. 3), lath-like and nearly square, ca. 100 Å thick, extended chain lamellae, with the square lamellae having the central bump. As shown in the insets the central bumps are elongated (along one of the diagonals of the crystals), measuring ca. 200 × 600 Å. A slightly thickened region surrounds each nucleus. Although not originally applied to crystallization in the form occuring here, the Hoffman–Lauritzen theory, in its various ramifications, could be applicable, the end surface of acetoxy- and carboxy-groups having a considerably different surface energy than the side surfaces. *Unexplained, however, is why the molecules in the lamellae stop adding monomer at a length of ca. 100 Å.* As shown in the figure, overlapping lamellae are also 100 Å thick, even though the molecules would be aligned so that end-linking (polymerization) across the interface could easily occur, particularly in the liquid crystalline state. We have observed similar 100 Å chain lengths in single crystal lamellae in numerous other CTFMP polymers, of liquid crystalline, flexible chain and intractable types. In most cases the thickness is apparently independent of the time and temperature of polymerization, with the polymerization temperature often being well below the mesomorph-crystal transition temperature ($T_{m\text{-}k}$) or the melting point (T_m) of the resulting relatively short chains. *The problem is, therefore, not restricted to a single polymer.* Representative examples are: (a) liquid crystalline homo- and co-polymers — poly(2,6-oxynaphthoic acid) [12]; poly(*p*-oxybenzoate) (P*p*OBA)on mica) [13]; large P(*m*OBA/ONA) crystals [14]; poly(*p*-phenylene terephthalate) [15]; bromine side group polyesters [16]; phenyl side group polyesters [17]; P(*p*OBA/ONA) [18]; polyoxybibenzoate [19]; (b) flexible chain polymers — poly (ethylene naphthalate) [20]; poly (butylene terephthalate) [21]; poly(ethylene terephthalate) [22]; and (c) intractable anhydride polymers — poly (naphthalic anhydride) [23] and poly(terephthalic anhydride) [24].

3.2. Growth faces (lamella shape)

3.2.1. Linear variation in apex angle — BCMO

The presence of curved growth faces on high temperature, solution grown, LPE single crystals, and their theoretical explanation was discussed in detail in the literature about a decade ago (see Section III G of Ref. [5]). Of equal concern, in terms of mode of folding, should be the change of apex angle of BCMO crystals as a function of temperature of crystallization and solvent [7,25,26]. The acute apex angle of the BCMO crystals in Fig. 2 is ca. 60°. For isothermal crystallization temperatures in xylene from 55 to 121°C, the apex angle varied linearly from 50 to 76° with the growth faces being planar over the entire range. Fig. 4 shows BCMO crystals grown at 104°C in *n*-butyl acetate and then annealed at 162°C for 30 min (T_m = 173°C); annealing resulted in a roughening and thickening of the edges

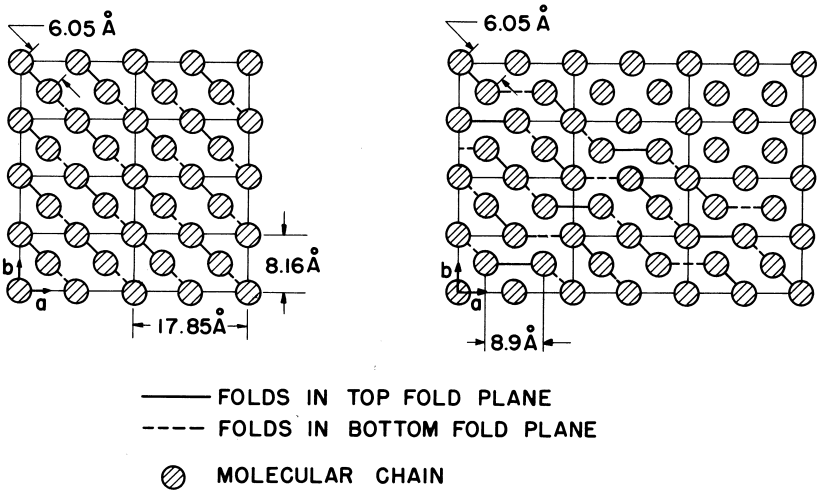

Fig. 6. Two-dimensional schematic representation of projections onto a 001 plane of the unit cell of BCMO single crystals. (a) Growth normal to {210} fold planes would result in an 85° apex angle. (b) Growth normal to {110} planes, by a 2/1 mixture of{210} and {010} folds would result in an apex angle of 49°. These represent the limits of the observed apex angles. Reproduced from Ref. [7].

only. The apex angle is 83°. The primary nucleus of the crystal on the left is visible just to the right of the large particle near the center. Both of these crystals again have the two "extra" layers although the crystal on the right has additional layers possibly originally growing at angles to each other.

Fig. 5 is a plot of the apex angle as a function of temperature of crystallization and solvent; similar variations were observed by Heber [25,26]. The two extremes in apex angle can be explained in terms of 110 and 210 fold planes, with the 110 fold planes requiring alternation of two 210 folds and one 010 fold for adjacent reentry (Fig. 6); the thickness of the crystals, as measured by SAXS from sedimented mats of the crystals [25,26] and from shadow lengths by TEM, agree and increased with crystallization temperature [7]. Not known is whether the molecular axes are tilted within the crystals as in hollow pyramidal LPE crystals; there is no apparent evidence for tilt. The linear change in apex angle appears to require a gradual change between the two types of folding. *There was (and is) no plausible explanation as to why the low crystallization temperature limit should involve a 2/1 mixture of types of folds, other than that it was related to the problems of packing regular, adjacent reentry folds on the fold surfaces, nor for the gradual change in angle.* More detailed study of these crystals is clearly warranted.

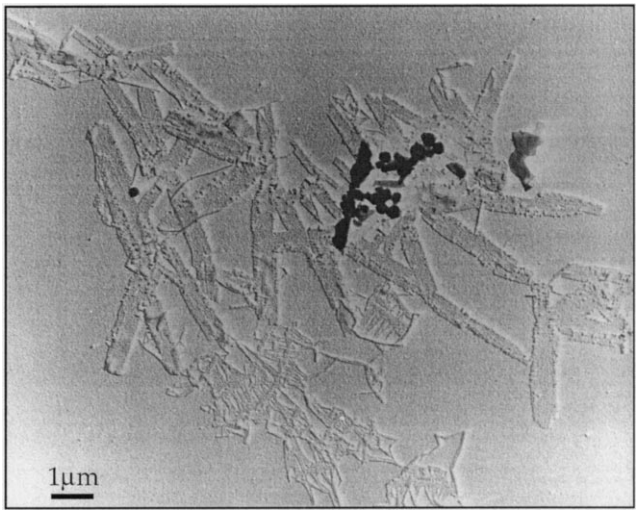

Fig. 7. Alpha-form single crystals of isotactic polypropylene crystallized from α-chloronaphthalene. Deformation resulting in fiber free cracks parallel to the long axis, fiber spanning micronecks normal to the long axis, was interpreted as indicating the fold planes were parallel to the long axis. Reproduced from Ref. [27].

3.2.2. Lath shaped crystals with irregular lath end growth faces

A somewhat different fold plane problem occurs in various ribbon- or lath-like crystals. We consider polypropylene [27] (Fig. 7), polyacrylonitrile [28,29] (Fig. 8), nylon 66 [30–32] (Fig. 9) and poly(β-hydroxybutyrate) (PHB) [33] (Fig. 10) crystals. For all of these the "growth faces" at the ends of the long axes are irregular and deformation evidence suggests the fold planes are parallel to the long axis. The problem here is that polymer crystal growth, in LPE for instance, occurs normal to the fold planes, fold planes stacking successively on each other as they are nucleated and fill out with folded chains. In the above four examples the growth is apparently parallel to the fold planes. Consistent with the jagged ends of the PP and PAN crystals, it is as if the molecule is folding only against itself in an isolated fold plane rather than having a "niche" to fold into. Such folding, however, would seem highly unlikely in these two polymers since the free energy gain of single fold plane folding must be small or positive. In the case of nylon 66 it could be somewhat larger (negative) since the H-bonds are made parallel to the long axes of the crystal. Indeed, Sakaoku et al., based on micrographs of nylon 66 crystals

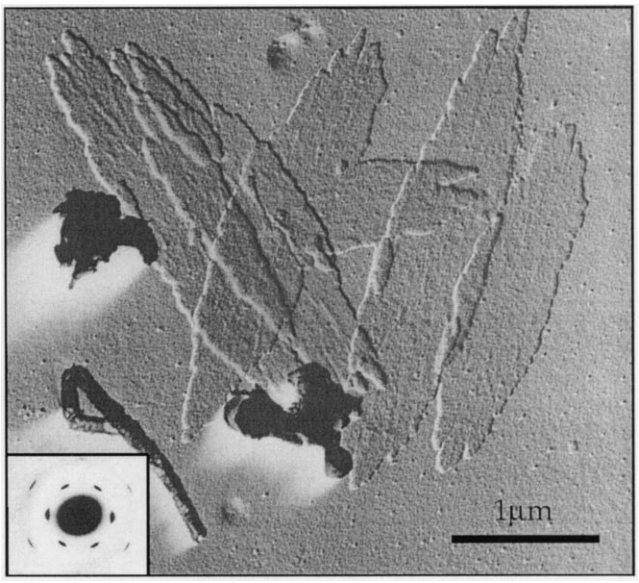

Fig. 8. Single crystals of polyacrylonitrile crystallized from a 0.5% propylene carbonate solution at 95°C for 3 days. An ED pattern is inset. Reproduced from Ref. [28]. Deformation of similar crystals on Mylar substrates indicated the fold planes were parallel to the long axis [29].

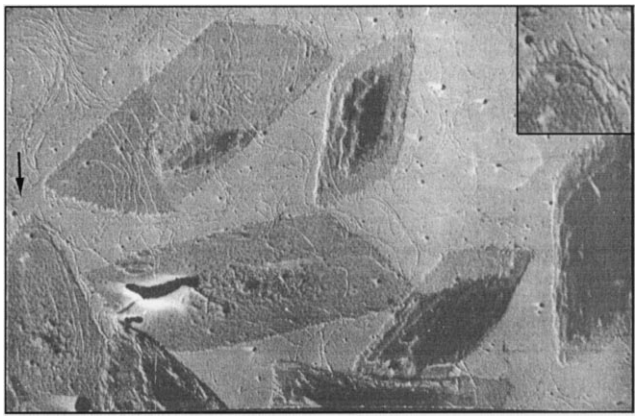

Fig. 9. Nylon 66 single crystals; crystallization conditions not known [32].

like that in Fig. 9 [32] suggested they formed by the lateral aggregation of "precursors", folded chain ribbons or fibrils. Kojima proposed a similar explanation for the growth of lath-shaped PP crystals [34].

Additional possible evidence for precursors was found in a study of the growth of PHB crystals from dilute xylene solutions [33]. The PHB was harvested from *Bacillus cereus* (ATCC 4342) grown in the lab. Fig. 10 shows low and high magnification views of typical crystals, here grown from 0.01% xylene solution at 100°C for 16 h (Fig. 10a) and 8 h (Fig. 10b) and subsequently "quenched" by spreading a small portion of the 100°C suspension on a carbon coated glass slide at room temperature (Fig. 10a) or −177°C (Fig. 10b), drying and preparing for TEM, after shadowing with Pt/C, by standard techniques. The crystals are lath-like in shape, as thin as 50 Å [35], with corrugations normal to the outer long edges on the 105 Å thick crystals shown here. PHB has a direction to its backbone, with the bacterial form being optically active, having two left-handed, anti-parallel helices in the orthorhombic unit cell [36]. The long axis of the lathes corresponds to the *a* axis, with folding expected to occur along 110 planes, the planes containing neighboring anti-parallel helices. Deformation of the crystals [33] confirms the fold plane orientation parallel to the long axis, fibers being pulled out across micro-necks when drawn parallel to the long axis and fiber-free cracks occurring when drawn normal to the long axis. As discussed by Birley et al., who described similar crystals of PHB and the copolymer poly(β-hydroxybutyrate/hydroxyvalerate) crystallized from a number of solvents [37], the molecules presumably fold on one fold surface along [110] and on the opposite surface [$\bar{1}\bar{1}0$], resulting in an average [100] fold direction. The PHB crystals they described, as in the original report [35], consisted of thin (40–60 Å) lathes without fold sectors or corrugations, tapering smoothly to sharp points. This shape further complicates any discussion of growth mechanism, the lateral face being at a slight angle to the 010 plane. With the molecular axes being normal to the fold surfaces and a crystallinity of >80%, the molecules must form regular, adjacent re-entry folds. The alternating fold directions were suggested as being related to the handedness of the molecules and the resulting special fold conformation.

Based on micrographs such as those in Fig. 10, it was suggested [33] that these crystals grew through the lateral aggregation of pre-folded ribbons or fibrils, one or only a few fold planes wide. Addition would be primarily at the ends, resulting in longitudinal growth parallel to the fold planes and jagged ends, and, to a lesser extent, on the lateral edges. We recognize, however, that ribbons of alternating 110 and $\bar{1}10$ folds seem unlikely. The possibility exists that the fibrils in Fig. 10 are the result of residual polymer in solution forming a very thin, negative staining type of film that shrank and split upon drying to form the fibrils, a possibility that might also explain the "precursors" in Fig. 9. *However, if one accepts the latter explanation, there still remains the problem of explaining lath-like crystal growth with fold planes parallel to the growth direction; we do not believe the growth of the above crystals can be explained by the presence of re-entrant faces or a small two-fold-domain growth face as for lozenge shaped PE crystals* (see Section III G of Ref. [5]) *or any other model that involves folding along fold planes that are normal to the*"*growth faces*" *at the ends of the laths* (e.g. Kyu et al. have recently proposed a model based on gradients of free energy normal to the growth faces that can lead to lath-like lamellae with flat short faces and flat or curved long faces [38]).

The corrugations are also of interest, suggesting that the crystals are non-planar, with the outside being larger than the inside. This is opposite to the case for hollow pyramids of LPE [39], which are larger on the inside and collapse with internal pleats and/or corrugations. With increasing time of

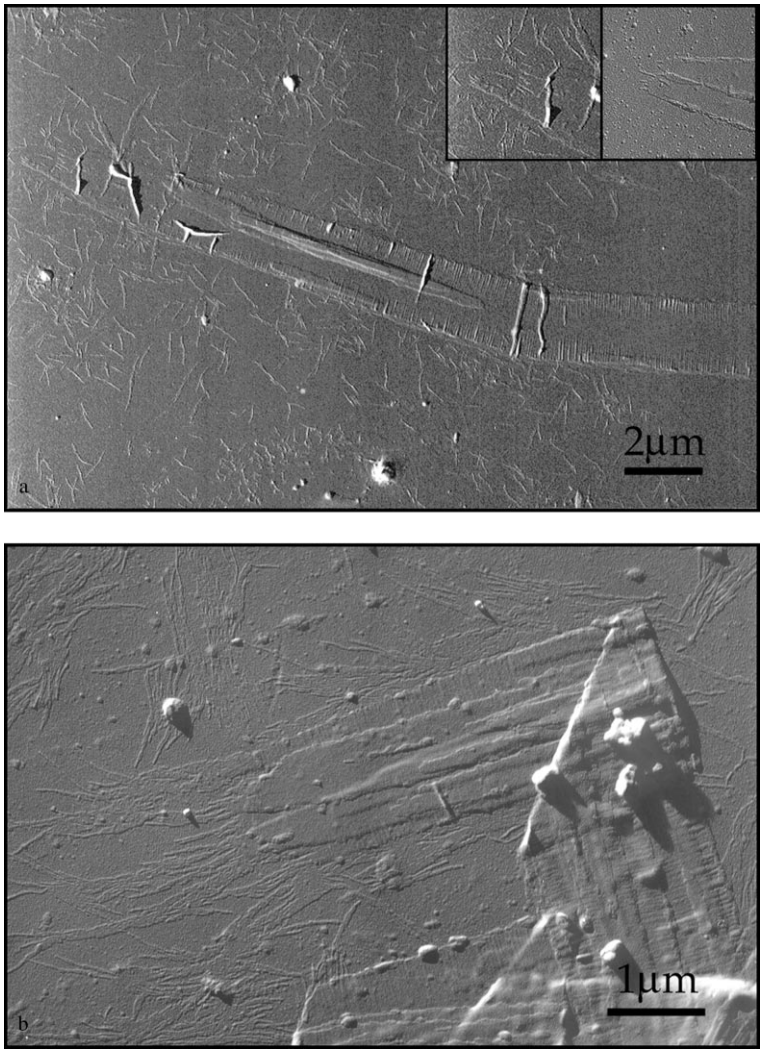

Fig. 10. Single crystals of PHB grown from 0.01 mole% xylene solutions at 100°C [33]. Preparation conditions are described in the text. The inserts in (a) are enlarged views of the ends of two of the crystals.

crystallization at 100°C, the corrugations disappeared, the crystals being flat when deposited. It was proposed that these crystals, in suspension, had an oscillatory, wavy ribbon shape, related to the form developed by a trimetallic strip, with a different metal on the edges (not surfaces) of the ribbon than in the center. Increase of the fold period in the interior of the crystal, following deposition of the fold planes, would result in its lateral shrinkage and the stresses leading either to helical or oscillatory twisting; a ca. 15% increase would yield the observed corrugations.

3.3. Lamellar doubling (free surfaces) and SAXS vs. TEM measurements of lamellar thickness for melt crystallized polymers

3.3.1. Lamellar doubling in polyethylene oxide — relation to SAXS periodicity

As shown by Barnes and Price [40] early in the days of the realization of lamellar crystallization of polymers from the melt, the lamellae observed on free surfaces of melt crystallized polymers can, in some cases, appear doubled. Fig. 11 is from a polyethylene oxide (PEO, Carbowax 6000, Union Carbide Chemicals Corp., Bound Brook, NJ) sample of molecular weight 12,000, crystallized isothermally at 56°C. The SAXS long period was twice the thickness, 200 Å, of the ca. 110 Å (eight folds) lamellar thickness obtained from the shadow lengths, both independent of the crystallization temperatures (48–56°C). The clearness of the doubling was less for a 50°C crystallization temperature, one of each pair appearing thinner with a less sharply defined edge. They suggested that the molecules were tilted in opposite directions in the pairs of lamellae. However, unless the interfaces in the center and outside of the pairs were of considerably different densities, alternating tilt would not be expected to result in doubling of the period. Furthermore, *hk*0 ED patterns were obtained from the lamellae indicating the regions diffracting had the molecules

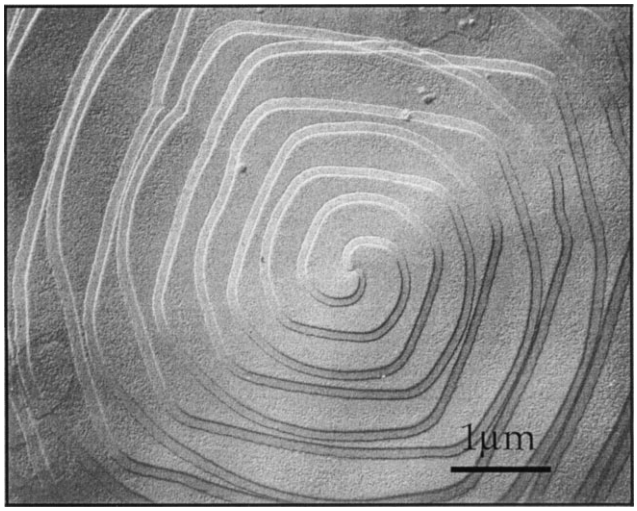

Fig. 11. Polyethylene oxide single crystal crystallized isothermally from the melt (see text) [40].

aligned nearly parallel to the normal to the lamellae; unfortunately, dark field micrographs were not taken and thus the extent of the diffracting regions is not known. *However, we have no acceptable explanation for the pairing or the doubling of the SAXS period.*

We have described apparently related, perhaps even less explainable in terms of current crystallization theory, observations for polyoxymethylene (POM) in which comparisons of SAXD and TEM lamellar thicknesses, lamellar doubling and interpretation of the SAXD spacings all have remaining questions [41–43]. We consider first the SAXD periodicities, as a function of crystallization conditions, and the relationship between them and the lamellar thicknesses as measured by TEM. This is followed by a discussion of the effect of annealing.

3.3.2. SAXS periodicities and relationship to TEM lamellar thickness measurements for as crystallized and drawn POM

For isothermally crystallized, slow cooled (3°C/min) and quenched (200°C/min) POM samples, 3.1 mm thick, the SAXS period (from slit- and Lorentz-corrected scans) was more than twice the observed lamellar thickness on free and, for the isothermally crystallized sample, fracture surfaces, based on replicas using latex particles for local shadowing angle calibration (Figs. 12a and 13a) [43]. The SAXS scans, for the isothermally crystallized sample (Fig. 13a) and a drawn sample, (Fig. 13b) show the effect of the various corrections. Although for the uncorrected curve in Fig. 13a the two inner reflections (with spacings ℓ_1 and ℓ_2, respectively, ℓ_2 corresponding to the periodicity of the second maximum) have a ratio ℓ_1/ℓ_2 of ca. 2, following the Lorentz correction (multiplication by θ) and a geometric correction to take into account the larger diameter of the ℓ_2 diffraction ring (also a multiplication by θ), ℓ_1/ℓ_2 is considerably less than 2 (1.6). Furthermore, in this sample the ℓ_2 reflection has a larger intensity than the ℓ_1 reflection.

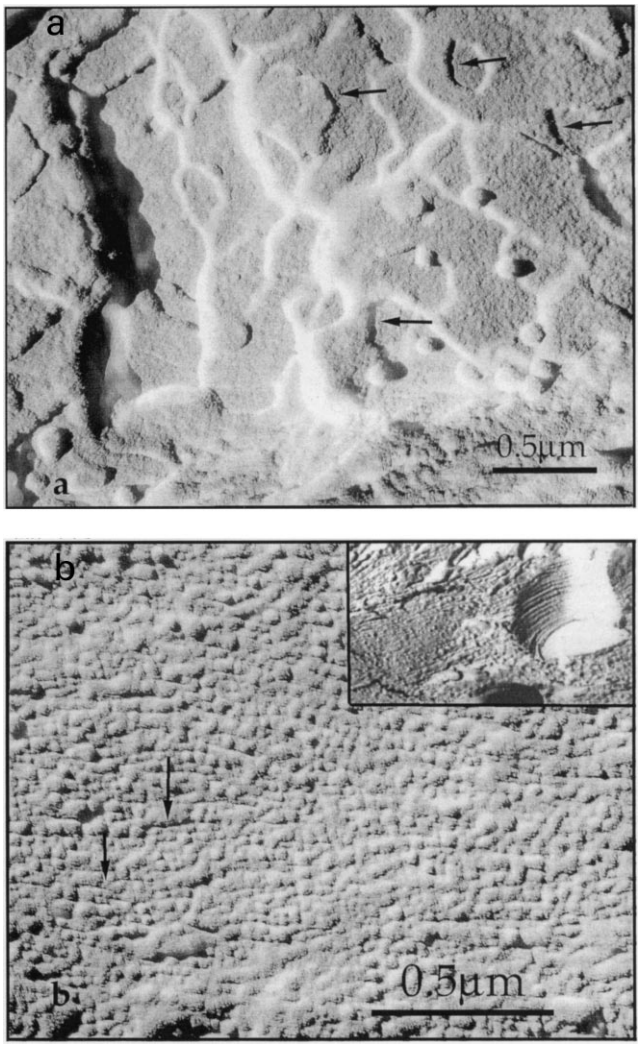

Fig. 12. Replicas of fracture surfaces of the isothermally crystallized POM sample used for the SAXS scan in Fig. 12. In (a) the fracture is interlamellar; in (b) it is ca. normal to the lamellae. Arrows indicate regions used for lamella thickness determinations [43]. The inset in (b) is from a similarly crystallized sample in which the "additive" has replicated the internal POM morphology, indicating the "bumpy" striations are due to lamellae normal to the fracture surface. The latex particles in (a) were used for local shadow angle calculation.

The correlation function $(\gamma_1(r))^2$ for this isothermally crystallized sample, using the corrected data, is shown in the inset; it has positive peaks corresponding to both ℓ_1 and ℓ_2. As described by Hsiao and Verma [45] and references therein (see also Ref. [46]), the thickness of the crystalline core ℓ_c and amorphous interface ℓ_a can be determined from the position of the first maximum (L_c^m) and the distance to the point the curve first crosses the r axis (B)

$$\ell_c = \{L_c^m \pm [(L_c^m)^2 - 4BL_c^m]\}/2 \quad (1)$$

[2] The correlation function is similar to the Patterson plot. The physical meaning can be visualized as the probability that a rod of a given length, with its end at a point in one phase, has its other end in a phase of the same density, as a function of the rod length [44].

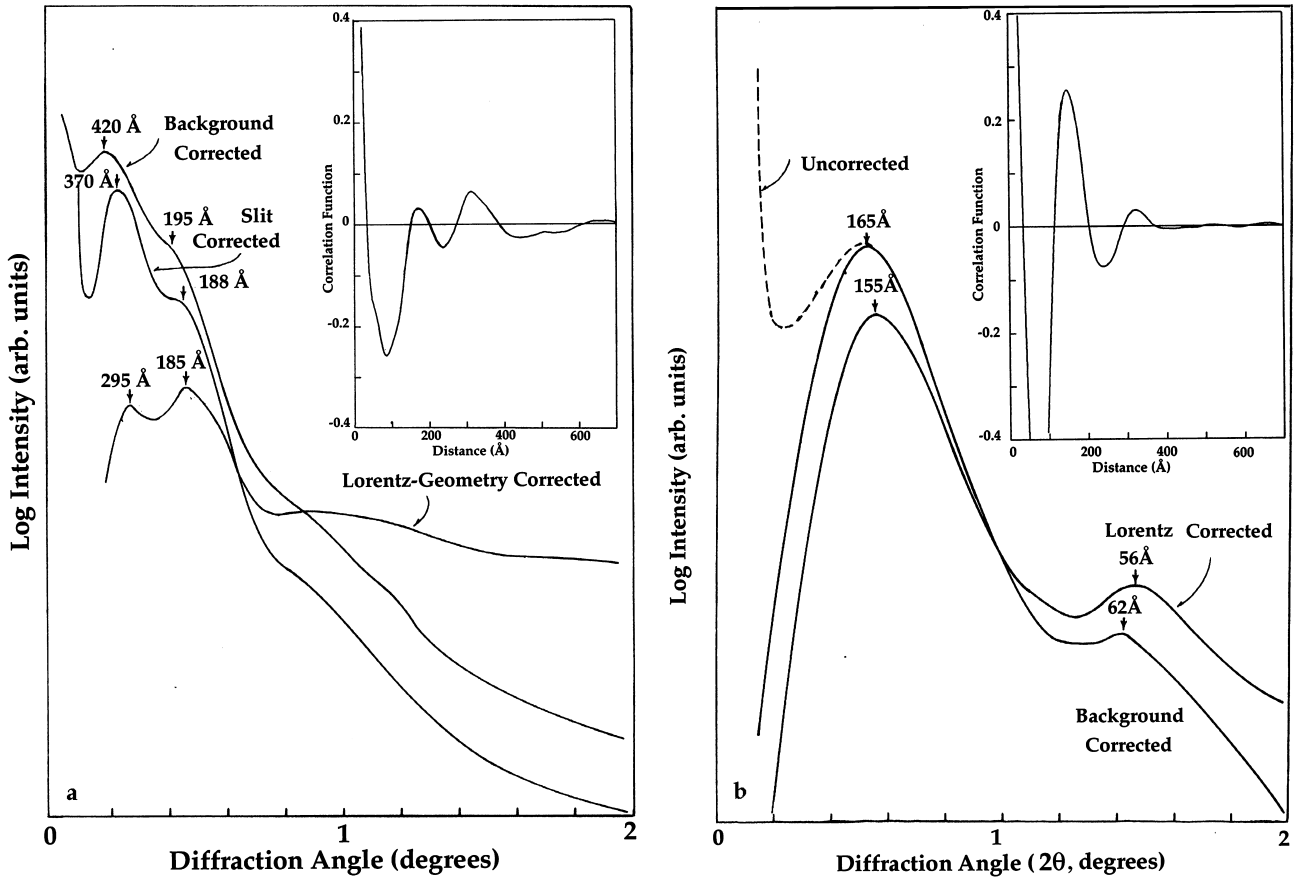

Fig. 13. SAXS scans from: (a) an isothermally crystallized sample of POM, and (b) a quenched sample drawn at 130°C and annealed taut at 163°C for 1 min. The patterns were taken with slit geometry, with the slit normal to the draw direction for (b). Correlation functions calculated from the corrected curves are inset [43].

$$\ell_c + \ell_a = L_c^m \tag{2}$$

where the sign in Eq. (1) has to be determined by other means, e.g. TEM. In the plots shown here for $\gamma_1(r)$ the intensity was measured out to angles where it was small relative to the intensity at the peaks, to reduce termination errors, but $\gamma_1(r)$ was not divided by the invariant Q [45,46] (the total integrated intensity), this being a constant for any given sample and not affecting the values of B and L_c^m (and thus ℓ_c and/or ℓ_a). Normally the first maximum of $\gamma_1(r)$, L_{c1}^m, is slightly smaller than ℓ_1 as determined by applying Bragg's law to the first peak of the corrected intensity and, if second-order "Bragg" reflections are present an L_{c2}^m may be present at twice the value of L_{c1}^m [45,46]. Here, however, the value of L_{c1}^m (169 Å) correlates with ℓ_2, ℓ_1 correlating with L_{c2}^m (312 Å). This is presumably due to the relative intensities of ℓ_1 and ℓ_2. It is noted $\gamma_1(r)$ can be interpreted as being due to a mixture of two different stacks of lamellae, one set having an average thickness related to L_{c1}^m with three "orders" (169, 345 and 510 Å) and the other set related to L_{c2}^m with two orders (312 and ca. 620 Å).

For the TEM micrograph shown in Fig. 12a the lamellar thickness, when the lamellae were parallel to the surface, was ca. the same as the ℓ_2 (L_{c1}^m) spacing in the SAXS scan; 140–170 Å vs. 185 (169) Å. On the other hand, on fracture surfaces of the same isothermally crystallized sample in Fig. 12a (Fig. 12b), the lamellar thickness of lamellae normal to the surface was ca. the same as ℓ_1 (L_{c2}^m) (220–320 Å vs. 295 (312) Å). Measurements for the "normal" lamellae were obtained from the thinnest periodicities observed on the fracture surfaces (arrows on figure) and from "internal replicas" resulting from a segregated additive that solidified below the POM crystallization temperature and replicated the internal POM surface against which it was in contact (see inset in Fig. 12b). The "beaded" nature of the edges of the fractured lamellae was attributed [43] to micronecking followed by fibrillar failure and retraction (melting?) despite the fracture being at liquid nitrogen temperatures, the fibrils being drawn out from individual lamellae. Fracture surfaces of the slow-cooled and quenched samples did not yield appropriate micrographs.

For the slow cooled sample (Fig. 14, with the effect of annealing, discussed below, also shown) the ℓ_2 spacing (59 Å) of the as-crystallized sample was also in agreement with the observed thickness of parallel lamellae on free surfaces (55–85 Å, Figs. 30a and 31a in Ref. [43]) whereas ℓ_1 was 160 Å. The corresponding value of L_{c1}^m was 159 Å,

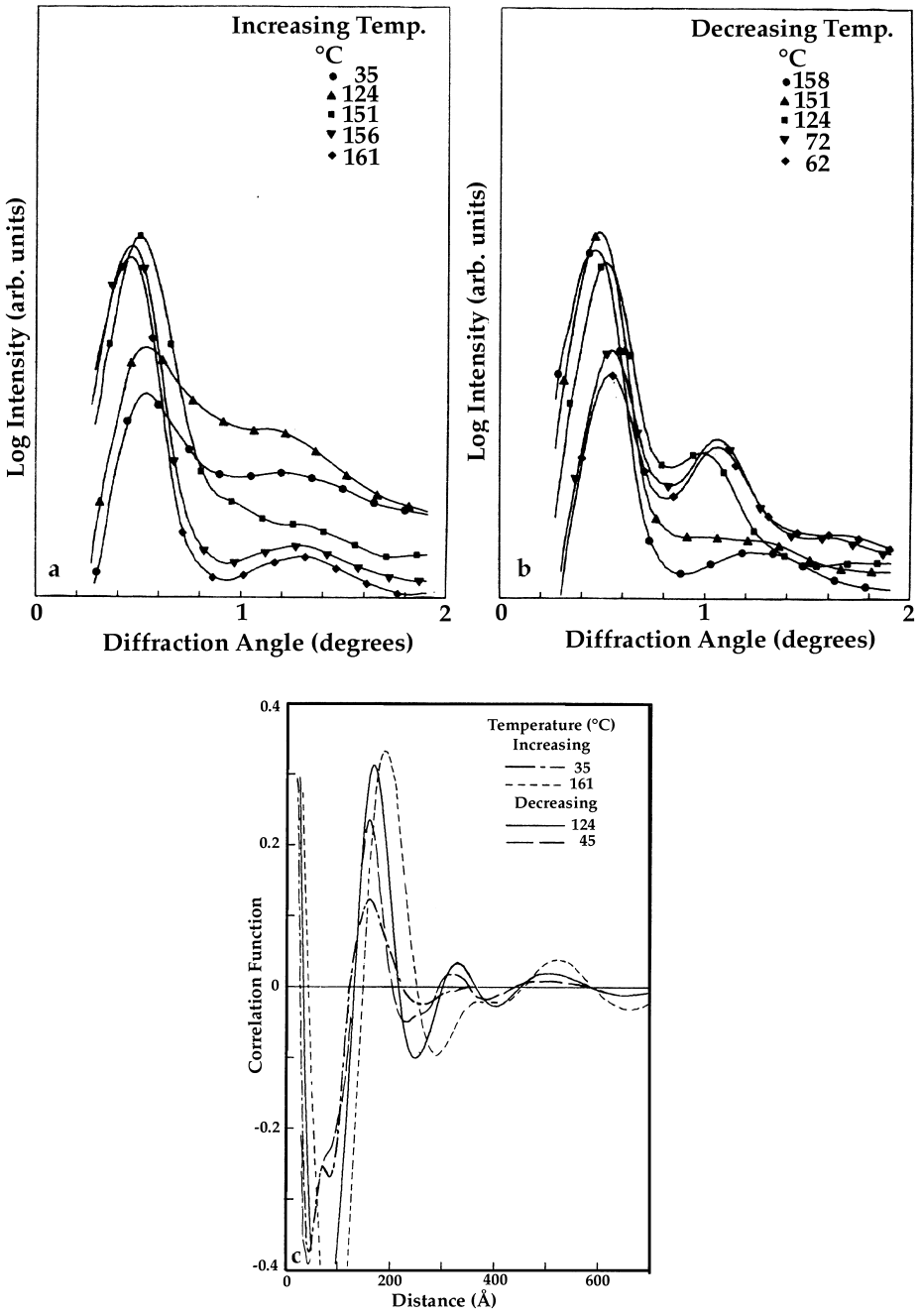

Fig. 14. SAXS scans taken during: (a) heating, and (b) cooling a slow cooled (3°C/min, ca. 3 mm thick) POM sample. Correlation functions for several of the scans are shown in (c) [43].

with L_{c2}^{m} not calculated. There is, however, a small peak at ca. 70 Å which may be related to the free surface lamellar thickness, again suggesting stacks of lamellae of two different average thicknesses.

For the quenched sample the lamellar thickness on free surfaces was 30–50 Å, with SAXS spacings of 142 and 56 Å (Fig. 15). Correlation functions were not calculated for this sample. The drawn sample (Figs. 13b and 15) was initially quenched, drawn at 0.05 in./min to its natural draw ratio at 130° C and then annealed taut at 163°C for 1 min. Surface replicas indicated it consisted of lamellae 100–130 Å thick, oriented normal to the draw direction, agreeing reasonably well with the SAXS ℓ_1 spacing (155 Å); ℓ_2 was 55 Å with $\gamma_1(r)$ maxima at 148 and 325 Å (Fig. 13b). Not known is whether there is a subsidiary maximum related to ℓ_2 in the first minimum, as in Fig. 14c.

In addition to the lack of agreement between the observed free surface lamellar thickness and the ℓ_1 value for both as-crystallized samples, ℓ_1/ℓ_2 was considerably larger than 2: 2.5 and 2.7, respectively (2.8 for the drawn sample). The ℓ_1/ℓ_2 ratios were even larger before correction (for the slow

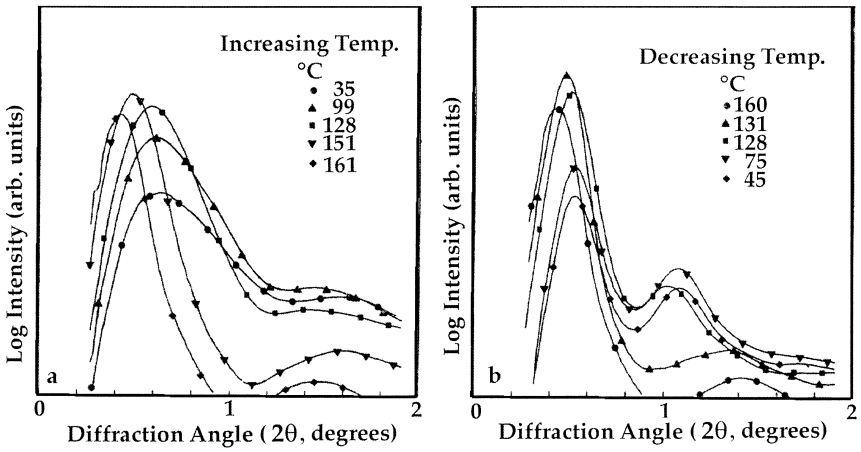

Fig. 15. SAXS scans taken during: (a) heating, and (b) cooling a quenched (ca. 200°C /min, ca. 3 mm thick) POM sample [43].

cooled sample: 3.8 before slit correction and 3.4 before the Lorentz-geometric correction). If they were first- and second-order reflections from the same structural elements the ratio should be close to 2. There are several possible explanations for the ℓ_1/ℓ_2 ratio being different than 2. Recent studies of LPE and POM samples suggest that it could be explained, as above, in terms of ℓ_1 being due to stacks of dominant (primary) lamellae and ℓ_2 to stacks of infilling (secondary) lamellae [47,48]. The other explanation can now be interpreted somewhat similarly, with the dominant and infilling lamellae being interspersed. Reinhold et al. [49] and subsequently Crist [50], based on paracrystalline disorders of the second kind, indicated that the ℓ_1/ℓ_2 ratio could differ from 2 if the distribution of lamellar thickness were skewed by an asymmetry parameter γ. γ is defined such that the maximum in the distribution of lamellar thicknesses is displaced from the average thickness by $(1-\gamma)$. The values for γ for the samples considered here were -0.32 for the isothermally crystallized sample and $+0.35$ to 0.50 for the slow cooled, quenched and drawn POM samples. *Although in great need of further correlated TEM and SAXS characterization, the skewed distribution explanation may explain the ℓ_1/ℓ_2 ratio for the drawn, annealed sample, for which the TEM observed thickness is in reasonable agreement with the ℓ_1 value, with the two types of stacks' explanation applying to the as-crystallized samples. However, neither of these explanations for the ℓ_1/ℓ_2 ratio can explain why the observed lamellar thickness in the as-crystallized samples agrees with ℓ_2.* We can only suggest that the lamellae observed on the fracture surface (parallel lamellae) and the free surface correspond to the secondary lamellae. We note that POM is a better sample than LPE for the proposed characterization in terms of both the greater sharpness and more orders of the SAXS scans and the self-etching of melt crystallized free surfaces.

3.3.3. Related observations for PE and polychlorotrifluoroethylene

The discrepancy between ℓ_1 and the lamellar thickness on surfaces is not limited to POM. Also described in Ref. [43] are SAXS and TEM results for a quenched LPE sample. The distribution of lamellar thicknesses on the surface, using the latex calibration, was centered at ca. 80 Å; the slit corrected SAXS spacings were 325 and 119, 260 and 112 Å after the Lorentz-geometric correction. In an earlier report [51] we compared the SAXS spacings, using uncorrected slit (and pinhole) collimation, and TEM measured free surface lamellar thicknesses for quenched, rapidly cooled and slow cooled samples; comparison of the SAXS patterns for samples of various thickness [52] indicated the discrepancy between ℓ_1 and the lamellar thickness on surfaces was not due to only surface lamellae contributing to ℓ_2. Values obtained were $\ell_1 = 210$ (195), $\ell_2 = 65$ Å, TEM = 60–70 Å for the quenched sample, $\ell_1 = 250$ (210), ℓ_2 not detected, TEM = 100–120 Å for the rapidly cooled sample and $\ell_1 = 295$ (240), $\ell_2 = 130$ Å, TEM = 130–150 Å, with the pinhole collimation values given in parentheses. Similar discrepancies were also reported for polychlorotrifluoroethylene [51] and, by others, for polyethylene [53,54].

3.3.4. Effect of annealing on the SAXS spacings and their relationship to TEM measurements in POM

The situation becomes more complicated when one examines the effect of annealing. For both slow cooled and quenched POM samples (Figs. 14 and 15), as well as a drawn sample (Fig. 16), heating followed by cooling on a heating stage in the SAXS system resulted in ℓ_1 increasing with both a reversible and irreversible component, the irreversible component depending on the original crystallization conditions and the maximum heating temperature (Fig. 17). The intensity went through a maximum during both the heating and cooling (Fig. 18). These results for $\ell_1$were interpretable [43] in terms of the suggestions of Fischer et al. [55–57] of a surface premelting for similar observations during annealing of bulk melt crystallized LPE, the crystal core becoming thinner than the interface thickness while heating and then rethickening during cooling. For the

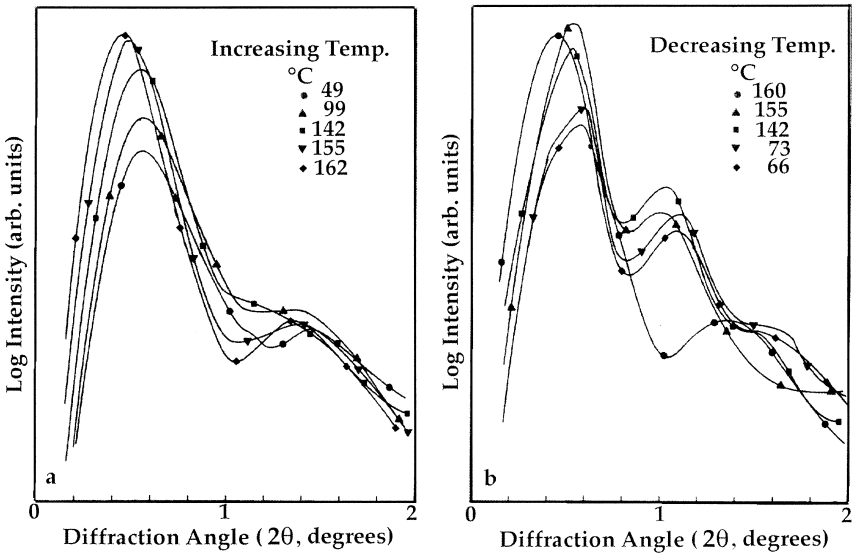

Fig. 16. SAXS scans taken during: (a) heating, and (b) cooling the drawn POM sample. The corresponding correlation function for the room temperature scan is shown in the inset in Fig. 12 [43].

quenched sample there is, in addition, an irreversible increase in thickness similar to that observed during the annealing of solution grown single crystals of LPE [58]. Taking into consideration the (different) increase in specific volume of both the amorphous and crystalline regions at elevated temperatures, the observed 17–18% reversible increase in ℓ_1 at the maximum in the ℓ_1 intensity (at which temperature $\ell_c = \ell_a$) for the slow cooled, quenched and drawn samples was explained in terms of conversion of crystalline material on the lamellar surfaces to amorphous. This is also in agreement with WAXD 009 line broadening measurements of a quenched sample during heating and cooling (Fig. 19). The initial increase in crystal thickness seems to correspond to the irreversible increase in ℓ_1, with the crystal thickness in subsequent cycles decreasing by 45 Å during heating and then increasing during cooling, reversibly. It was noted that the changes in ℓ_1 occurred above 145°C, ca. the temperature of the α relaxation in POM which is interpreted in terms of the onset of molecular rotation and translation in the crystalline regions [59,60].

However, ℓ_2 followed a different path (Fig. 20); for the slow cooled sample ℓ_2 remained nearly constant to the maximum temperature, with the intensity decreasing, and also during cooling, down to at least 150°C. At 124°C, the next temperature at which the pattern was measured, ℓ_2 had *increased* by ca. 20 Å, to 90 Å (which is close to 1/2 the

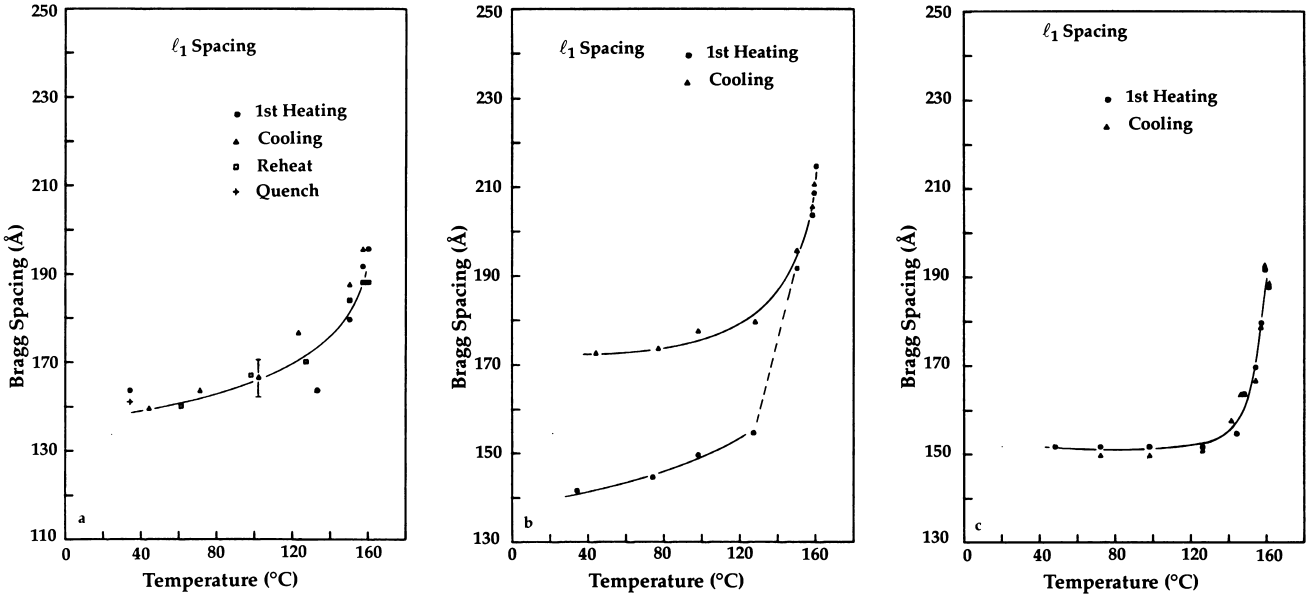

Fig. 17. Plots of the ℓ_1 spacing vs. temperature during the heating and cooling scans for the: (a) slow cooled, (b) quenched, and (c) drawn POM samples. The lines are drawn through the cooling points [43].

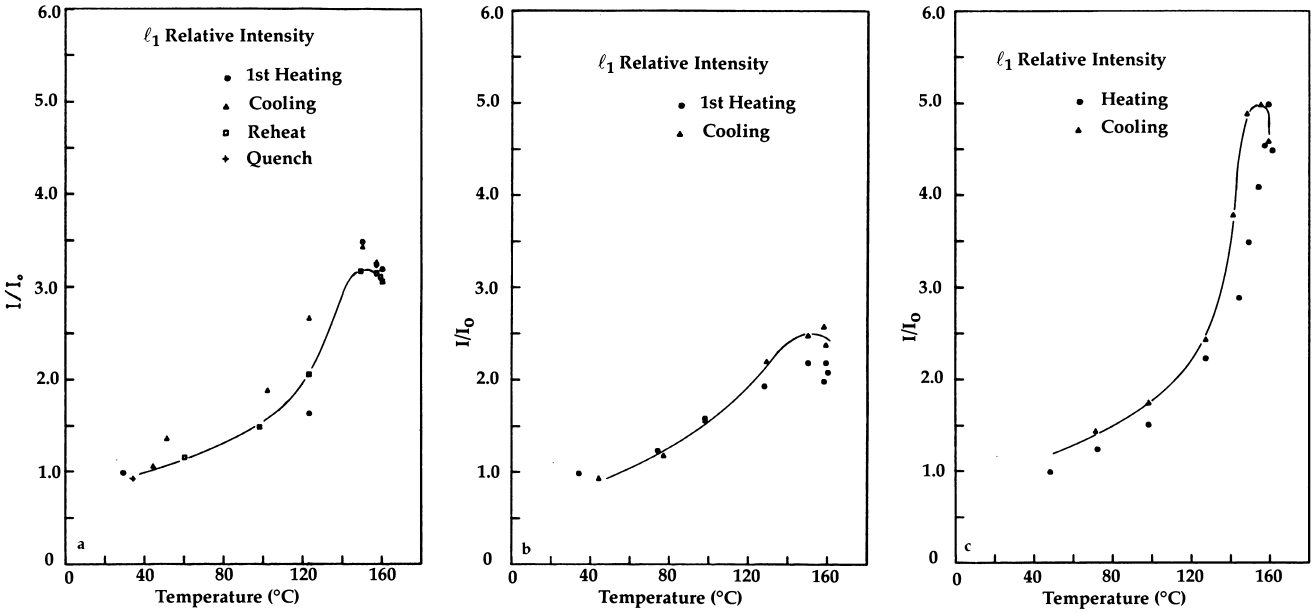

Fig. 18. Plots of the relative intensity of the ℓ_1 maximum vs. temperature during the heating and cooling scans for the: (a) slow cooled, (b) quenched, and (c) drawn POM samples. The lines are drawn through the cooling points [43].

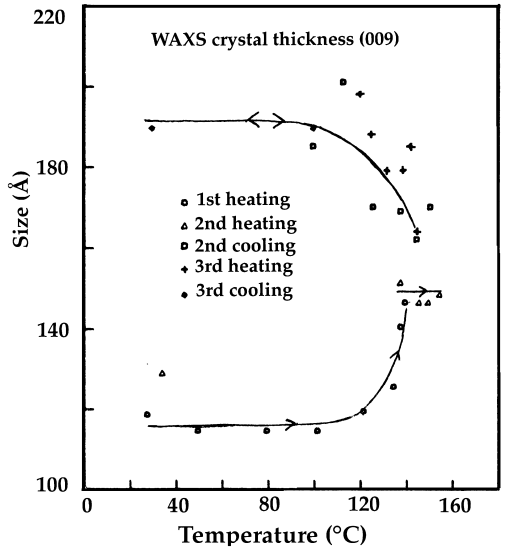

Fig. 19. Crystal thickness of quenched POM as a function of temperature during several cycles of heating and cooling. The first heating scan was terminated at 130°C, due to equipment failure, with the sample being rapidly cooled to room temperature, with a decrease in crystal thickness from 145 to 130 Å. It was then reheated rapidly to138°C during the second heating scan, the thickness returning to 145 Å. Further heating to 155°C resulted in no change in thickness. Cooling from 155 to 100°C (first cooling) resulted in an *increase* in crystal thickness to 187 Å, corresponding to the irreversible increase in ℓ_1. Subsequent heating and cooling to room temperature resulted in reversible decreases (during heating) in ℓ_1, from 187 to 160 Å. Simultaneous with the *decrease* in crystal thickness, ℓ_1 *increased* from 176 to 189 Å [43]. The decrease in crystal thickness is recognized as being too small to lead to the maximum in ℓ_1 intensity in Fig. 17.

value of ℓ_1 at the same temperature (ca. 176 Å) This ratio was retained during further cooling and a subsequent heating and cooling scan in which the original maximum heating temperature was not exceeded. Similar results were obtained for both the drawn and quenched samples during first heating. ℓ_2 increased only slightly during cooling of the quenched sample from 162 to 131°C, followed by an increase of ca. 20 Å at 128°C. The drawn sample increased by an even larger amount when cooled from 160 to 155°C. In all three samples the "new" ℓ_2 is considerably sharper and higher in intensity than the old and the ℓ_1/ℓ_2 ratio is ca. 2.0 (see Fig. 23, Ref. [43]). A third-order reflection is even seen for all three samples after cooling to room temperature indicating a high degree of perfection in the thickness of the lamellae. For three orders of reflections the paracrystal diffraction theory [61] requires that the standard deviation of a Gaussian lattice spacing distribution function, divided by the average lattice spacing be less than 12 Å. It is these results that led us originally [43] to suggest that the $\ell_1$and ℓ_2 of the as-crystallized samples were due to stacks of lamellae of two thicknesses rather than interspersed lamellae and that ℓ_1 and ℓ_2 were not related; whether ℓ_2 remains after the heating and cooling cycle, being "buried" under the new ℓ_2 or the corresponding lamellae totally melted and were converted to the thicker lamellae could not be determined from the SAXS patterns.

Interpretation of the correlation functions was not discussed in the original publication [43]. The correlation functions corresponding to some of the scans for the slow cooled sample are shown in Fig. 14c. L_{c2}^{m} for the three samples for which it was determined are at values ca. twice that of L_{c1}^{m} with a "third-order" also being seen for these samples. For both low temperature samples, before

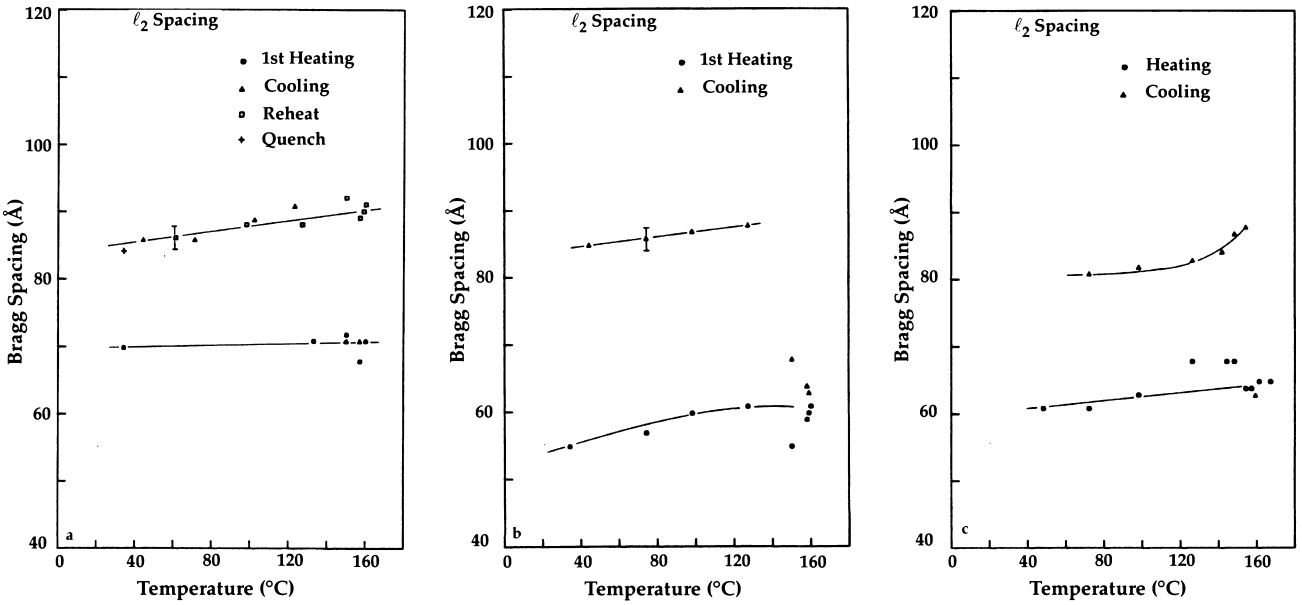

Fig. 20. Plots of the $\mathcal{L}_2$ spacing vs. temperature during the heating and cooling scans for the: (a) slow cooled, (b) quenched, and (c) drawn POM samples. The lines are drawn through the cooling points [43].

and after heating, an additional small peak is seen at small values of r (ca. 70 Å), close to the values of $\mathcal{L}_2$ (59 Å) before heating. This is despite the fact that after heating $\mathcal{L}_2$ had increased significantly, to ca. 85 Å, now ca. 1/2 the value of $\mathcal{L}_1$. The retained presence of the 70 Å peak could, as suggested above, be due to the reflection due to original stacks of thin lamellae being "buried" under the new second-order $\mathcal{L}_2$ of the stacks of thick lamellae; this would also require that they not fully melt at the maximum temperature and recrystallize as thicker lamellae during cooling. For this sample, assuming one accepts all of the corrections made to the scans and the basis for the calculation of Eq. (1), $\mathcal{L}_c$ remains nearly constant during the heating and cooling, the change in $\mathcal{L}_1$ and L_{c1}^{m} being due solely to changes in $\mathcal{L}_a$. This cannot be explained in terms of surface melting, which would reduce $\mathcal{L}_c$ as $\mathcal{L}_a$ increased. In terms of the method of calculating $\gamma_1(r)$ this would require a larger increase in B than that observed. *Characterization of the correlation functions for all of the types of samples is needed, including drawn samples.*

Obviously of interest would be following the changes in the lamellar structure on a surface of a sample by microscopy as it is heated and cooled. Although at the time of these experiments there was no possibility of following the changes in lamellar thickness by microscopy (scanning probe microscopy, with a heating stage would permit such observations at present), the changes were followed by repeat replicas before and after the heating cycle and at the maximum temperature. The identical areas of the sample were identified by combining optical and electron microscopy of replicas prepared by Pt/C shadowing at room temperature or on a hot stage in the vacuum evaporator, followed by stripping with polyacrylic acid at room temperature. The high temperature replica presumably faithfully reproduced the topography at the shadowing temperature, no significant cracking being observed. Calibration with latex was not possible so lamellar thicknesses could not be measured on the micrographs. Fig. 21 shows replicas of the same area of a sample before and after annealing at 157°C, 5 min. This sample had been previously drawn 20% at 128°C, resulting in the drawing out of "interlamellar links" between lamellae oriented parallel to the surface in the micrograph shown in Fig. 13, Ref. [42] due to interlamellar shear. In the micrograph shown in Fig. 21 [62] interlamellar shear was negligible. Other similar micrographs of undrawn samples are shown in Figs. 30 and 31 of Ref. [43]. The initial SAXS Bragg lamellar thickness of this sample was 140 Å, increasing to 149 Å after annealing (uncorrected data). In addition to retraction of the interlamellar links during the relaxed annealing [42], there is a clear ca. doubling of the number of visible lamella edges in both of the regions shown in Fig. 21. This also occurred in both samples shown in Ref. [43], with no apparent change between the micrograph taken after annealing and subsequently at the annealing temperature. *We are thus left with the problem that if $\mathcal{L}_2$ is due to stacks of infilling lamellae and are the lamellae seen on free surfaces, the SAXS results require that they either disappear during the annealing, recrystallizing as new $\mathcal{L}_1$ lamellae, or remain on the surface (with their SAXS periodicity "buried"). For either explanation how can the number of lamellae on the surface double?* Here we can only suggest, as in the case of PEO crystallized at 50°C, that they are actually present initially but that their edges are only poorly visible. The insert in Fig. 21a is a magnified image of a portion of the figure with the locations at which the "new lamellae" become visible

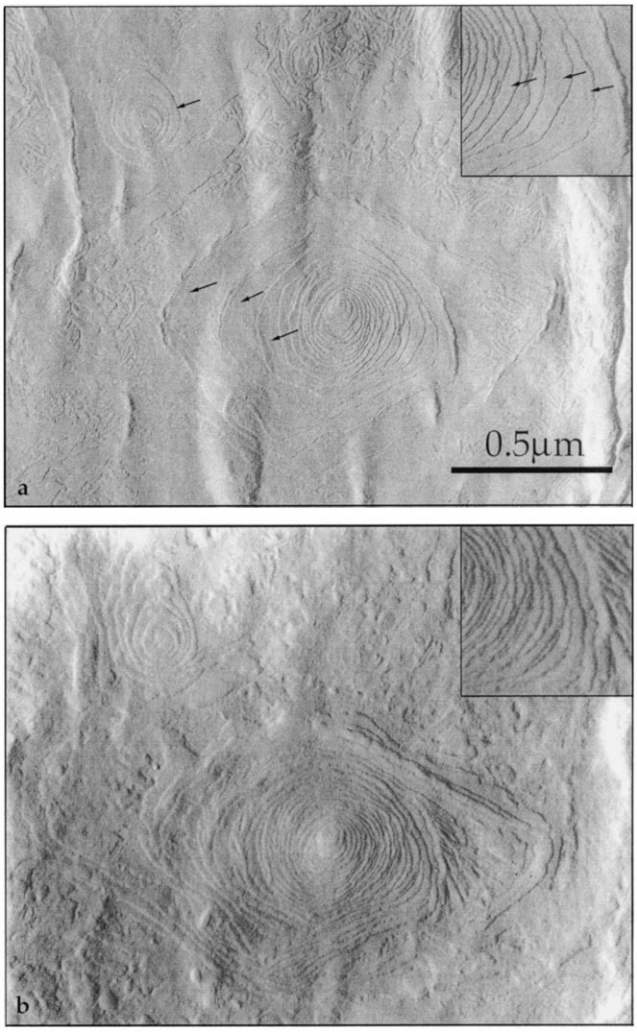

Fig. 21. Repeat replicas of a POM sample crystallized with a free surface by slow cooling, (a) before, and (b) after annealing at 157°C for 5 min. Arrows indicate regions in which thin, "lamellar edges" are just barely visible before annealing, but, after annealing, have the same apparent thickness as the lamellae originally clearly visible [62].

indicated by arrows. *This suggestion, however, still does not yield an explanation of the SAXS spacing for PEO being in agreement with the double thickness.*

To summarize:

1. POM can show both a reversible and irreversible change in $\mathcal{L}_1$ (and L_{c1}^{m}) spacing and intensity in a heating and cooling cycle, with the irreversible component depending on the initial crystallization conditions and the maximum heating temperature; second cycles are completely reversible if the original maximum temperature is not exceeded. The magnitude of our results can be explained in terms of the changes in density of the amorphous and crystalline regions as a function of temperature and Fischer et al.'s. surface melting model [55–57] (for details see Refs. [40,43]). We note that we do not believe melting of thin, secondary lamellae between the dominant lamellae, as proposed for explaining changes in $\mathcal{L}_1$ for poly (aryl ether ether ketone) [63], can explain the results for POM; these interspersed lamellae cannot be present in the annealed samples for which 2–3 "true" orders of reflections were obtained that changed reversibly in both intensity and spacing during heating and cooling and the increased spacing in the once heated sample is too small (none in the slow cooled sample) to permit incorporation of the thin lamellae in the thick ones. Rather, based on the $\gamma_1(r)$ plots, it appears that large (giving rise to several orders of L_{c1}^{m}) stacks of both thick and thin lamellae are present. However, similar effects are seen in the drawn sample and we know of no suggestions for similar, two periodicity, populations of lamellae in this type of sample.
2. $\mathcal{L}_1/\mathcal{L}_2$ can be either larger or smaller than 2 in as-crystallized samples; again this can be explained as scattering from stacks of thick dominant lamellae ($\mathcal{L}_1$) and thin, secondary lamellae ($\mathcal{L}_2$) but with only the secondary being observed on free surfaces (POM and LPE) and fracture surfaces in which the lamellae are parallel to the fracture surface (POM). We do not believe it can be due to a distribution of lamellar thicknesses within a stack (paracrystalline disorder of the second kind, due to interspersed infilling lamellae).
3. $\mathcal{L}_2$ shows essentially no change as an as-crystallized sample (for all three types) is heated and *during the initial stages of cooling*, with the intensity decreasing during heating, particularly above ca. 140°C (ca. the α relaxation temperature [43]) and increasing during cooling. *If $\mathcal{L}_2$ is from separate stacks we have no explanation for the changes in intensity unless $\mathcal{L}_a$ is already larger than $\mathcal{L}_c$ at room temperature.* The disappearance of the original $\mathcal{L}_2$ part way down in the cooling cycle, we suggest, is because it becomes hidden by the increase in perfection of the stacks of dominant lamellae giving rise to the strong "true" second- (and third-) order reflections.
4. Micrographs before and after annealing show a doubling of the number of lamellae on free surfaces with no apparent increase in thickness (or decrease). Traces of the "new" lamella edges can be seen on the initial surfaces. *Here we can only suggest that caution is required in interpreting free surface micrographs in terms of internal structure.*
5. For the drawn, annealed sample, for which $\mathcal{L}_1$ agrees with the observed lamellar thickness on the surface, an asymmetric distribution in lamellar spacings could be present, giving rise to the greater than 2 (2.8) $\mathcal{L}_1/\mathcal{L}_2$ ratio. The $\gamma_1(r)$ data is inconclusive; the first minimum is not fully plotted and thus the possibility of a subsidiary maximum, as in Fig. 14c (and possibly Fig. 13a), agreeing with $\mathcal{L}_2$ cannot be determined. The effect of annealing time and temperature, fixed and relaxed, is in need of investigation by both TEM and SAXS.

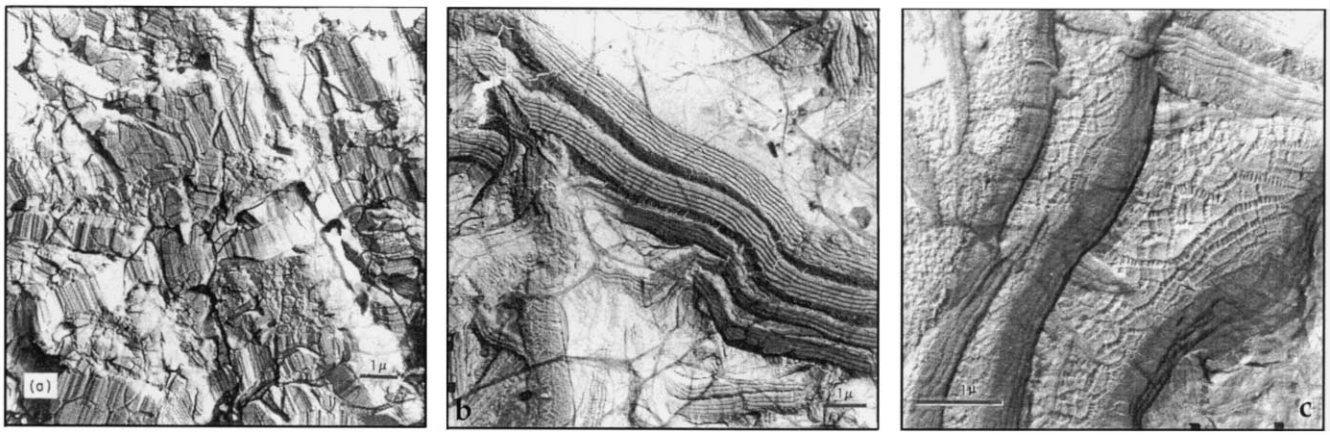

Fig. 22. Replicas of: (a) a fracture surface, and (b), (c) free surfaces of PTFE crystallized slowly from the melt [52].

3.4. Surface effects

3.4.1. Polytetrafluoroethylene

Related to the problems of lamellar doubling and the relationship between lamella observations on free and fracture surfaces are some old and recent studies of polytetrafluoroethylene (PTFE). It is well known that "banded" structures are present on fracture surfaces of PTFE crystallized slowly from the melt (Fig. 22a) (Ref. [52], see also Refs. [64,65]). This sample was prepared by compaction of PTFE dispersion particles at 380°C followed by slow cooling and fracture under liquid N_2. They are presumably chain extended crystals, resembling the extended chain crystals of LPE crystallized from the melt under pressure [66]. Free surfaces of similarly prepared samples consisted of bands with striations parallel to the long axes (Fig. 22b) and, apparently, thinner, folded chain lamellae (Fig. 22c) [52]. In agreement with the study of Melillo and Wunderlich of crystallization on PTFE fracture surfaces during annealing [67], the parallel striations could be interpreted as low molecular weight, extended chain or folded chain, oligomers crystallizing epitaxially on the chain extended surfaces of the bands. The folded chain lamellae in Fig. 22c could also be exuded, low molecular weight material. Less well known is that thin, folded chain single crystals of PTFE can be prepared from the melt by dispersing the dispersion particles on a substrate and heating to 350–380°C [68]. An example [69], using DuPont's 5070 nano-emulsion PTFE ($\bar{M}_n = 50,000$, chain length 1300 Å, particles nearly monodisperse, consisting of ca. 750 Å diameter hexagonal discs, 700 Å thick, as compared to ca. 2–3000 Å long ellipsoids for typical dispersion particles) melted at 350°C for 30 min and then slow cooled, is shown in Fig. 23. The lamellae lying on the substrate have a shadow length corresponding to a thickness of 100 Å and, as shown by the inset, frequently are doubled with the lamellar thickness being 1/2 that measured from the shadows. In addition, parallel striations are seen, presumably lamellae trying to grow normal to the substrate, which also often are doubled. We see nothing to suggest these striations result from epitaxial crystallization. By using somewhat "thicker" original films, structures presumably related to the bands can be grown [69] for both low molecular weight (Fig. 24a) and high molecular weight (Fig. 24b) PTFE. If so, they are always covered by the, often doubled, striations. Tending to suggest that epitaxy is not the origin of the striations is the observation that the individual pairs can extend out from the bands as single entities, sometimes appearing on top of apparent parallel lamellae (upper right of Fig. 24a) and sometimes with no apparent PTFE substrate (lower right of Fig. 24a). This can also be seen in Fig. 25, of a PTFE nano-emulsion heated at 350°C, 30 min and then slow cooled, in which the individual particles have developed a double striation appearance. The inset ED pattern, from the region indicated by the arrow, indicates that the molecular axes are in a plane normal to the striations; non-equatorial reflections were not observed in any similar pattern.

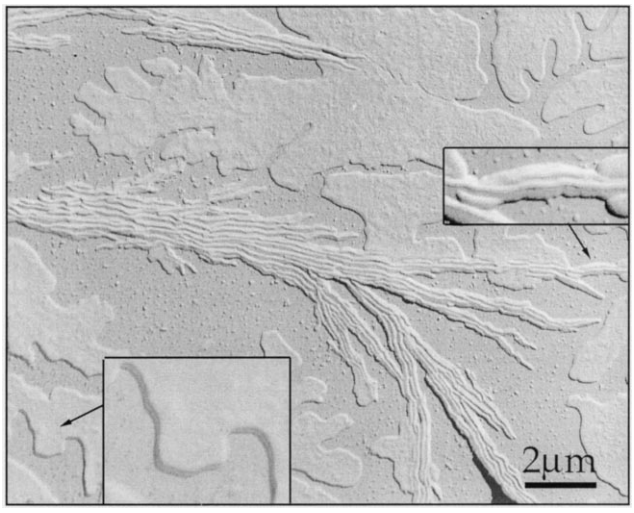

Fig. 23. Thin film of DuPont 5070 PTFE nano-emulsion crystallized from the melt (350°C, 30 min). The insets are enlarged views of the regions indicated by the arrows [69].

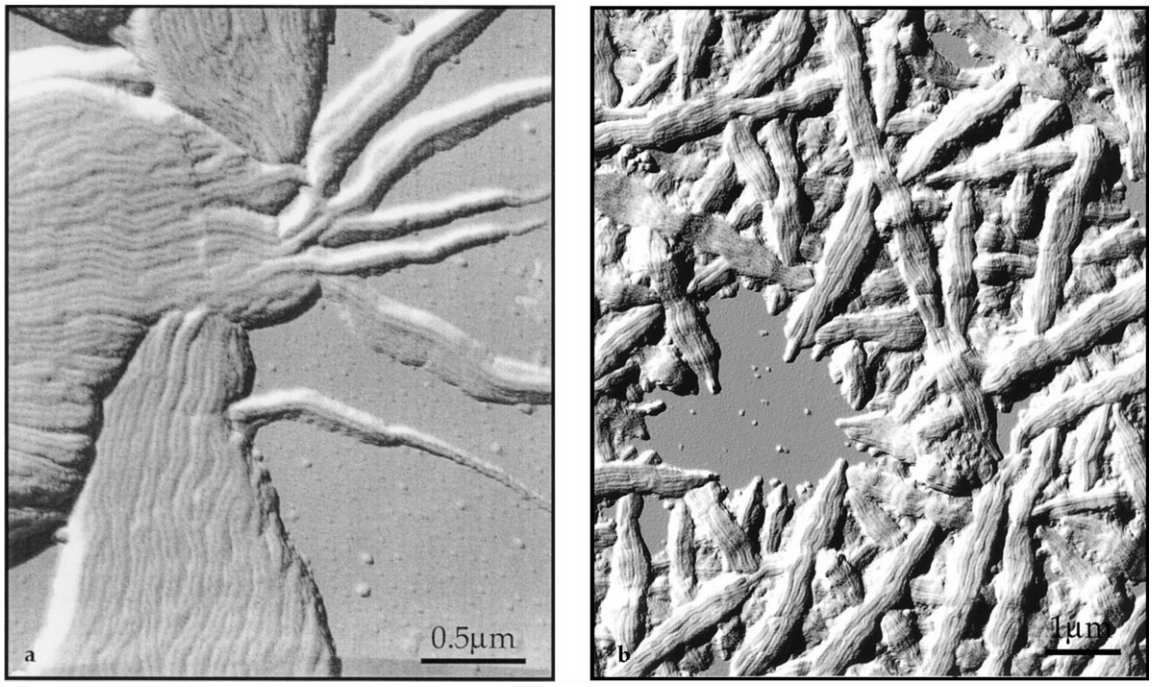

Fig. 24. Thin films of: (a) an Ausimont[3] nano-emulsion PTFE, and (b) Teflon[4] 30 emulsion particles crystallized from the melt (both 380°C, 20 min). The Ausimont particles are rods of variable length (up to 1500 Å) and diameter (200–400 Å), $\bar{M}_n = 200,000$. $\bar{M}_w = 49 \times 10^6$ number average chain length 5200 Å [69].

At this time we have no explanation for the doubling in PTFE or for the structure in between the striations; the fact that they are so easily seen in shadowed samples indicates a considerable valley is present between the two "lamellae". The chain folding in the single crystals and, apparently, on the free surface, we suggest is due to an as yet unexplained effect of the surface of the sample on the crystallization process. We also note that, if the listed molecular weights are correct, the PTFE is folded within the nano-emulsion particles, the DuPont 5070 and Ausimont particles apparently being single crystals with the molecules parallel to the axes of the Ausimont rods. *Of interest would be whether LPE crystallized under pressure, crystallizing from a "disordered(mobile) hexagonal phase"* [70], *would also show folded chain lamellae on a "free" surface after the rest of the sample has become chain extended or extended chain.*

3.4.2. Surface effects in a random liquid-crystalline-terpolymer crystallized from the liquid crystalline state

Although we know of no observations of free surfaces of pressure crystallized LPE, a related experiment can be, and has been, done by crystallizing a liquid crystalline (LC) polymer from the mesomorphic state. Fig. 26 shows the results of crystallizing a random, LC terpolymer polyester (composed of equimolar amounts of *p*-oxybenzoate, dioxyphenyl and flexible pimeolate residues) from the nematic state [71]. The interior consists of extended chain lamellae, the thickness distribution permitting determination of the molecular weight distribution; quenching resulted in thinner, chain extended lamellae. The free surface of the same slow cooled sample, on the other hand, consisted of 90 Å

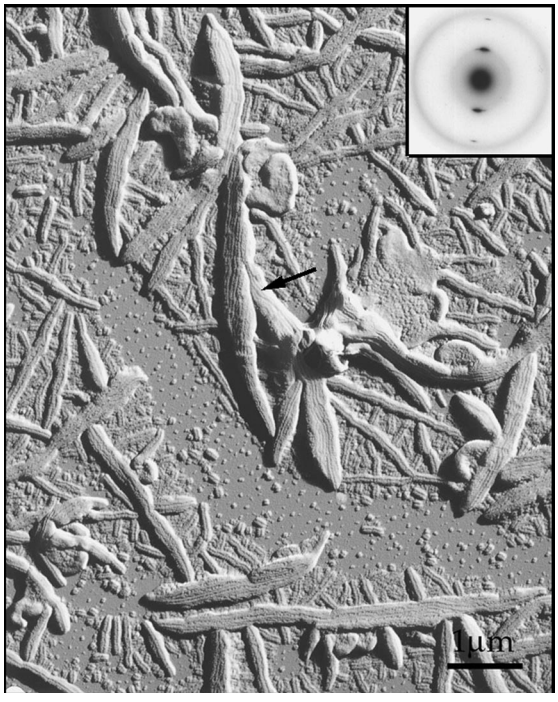

Fig. 25. Thin film of a PTFE nano-emulsion crystallized from the melt (350°C, 30 min) [69].

[3] Produced by Ausimont USA Inc., Thorofare, NJ.
[4] Trademark of E.I. DuPont de Nemours & Co. Inc., Wilmington, DE.

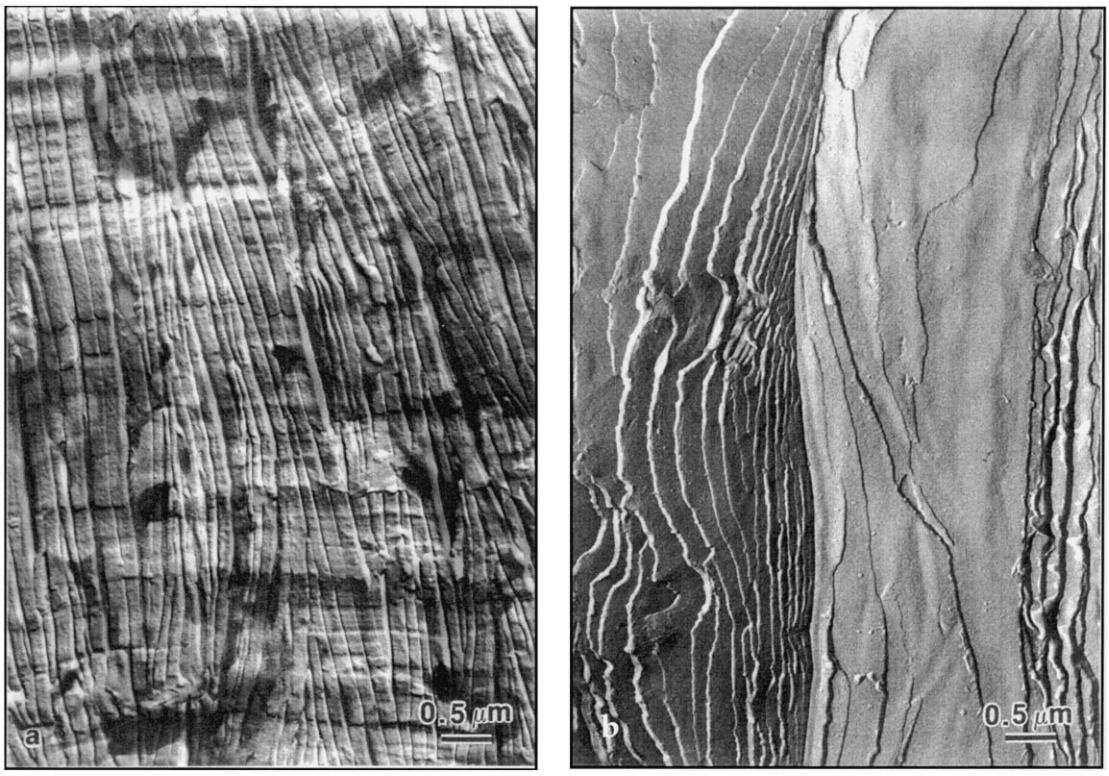

Fig. 26. (a) Fracture, and (b) free surfaces of a random 1/1/1 ter-polyester liquid crystal polymer, crystallized from the nematic state [71].

thick, presumably folded chain, lamellae. For this sample the average chain length corresponds to nine folds. Although it is possible that low molecular weight polymer has exuded to the surface, forming thin, extended chain lamellae, we believe they are folded chain lamellae.

Further evidence for a role of the surface in affecting the type of crystallization can be seen from the results of crystallizing the same polymer from the nematic state in thin films on a glycerin surface (Fig. 27) [72]. The fold period here is 70 Å, corresponding to five folds for the polymer used, with ED patterns showing the molecules to be normal to the lamellae. Similar, more irregular looking lamellae were grown in a similar fashion from the higher molecular weight polymer and from related terpolymers containing C_4, C_6 and C_7 flexible segments; the ones with even numbers of C atoms being more irregular than those with odd numbers.

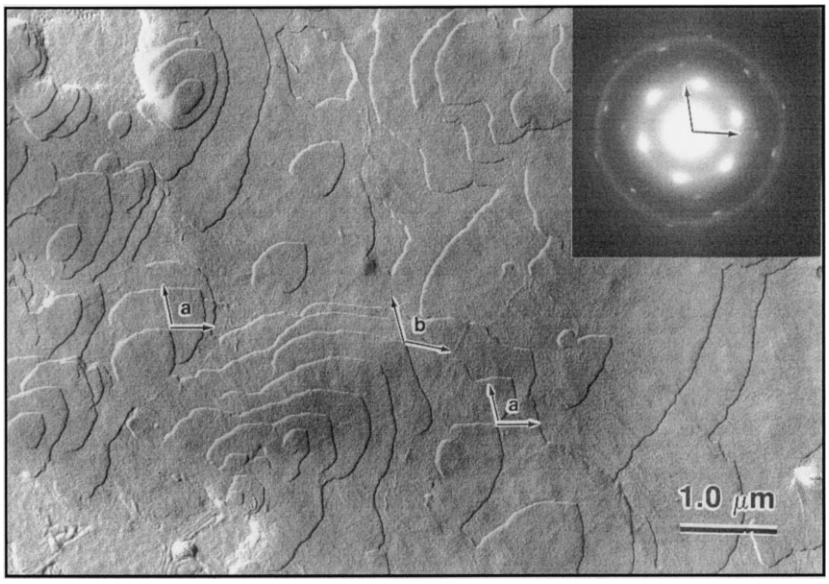

Fig. 27. Thin film of the random ter-polyester crystallized from the nematic state on a glycerin surface. The arrows indicate 210 fold plane growth faces [72].

It is noted that despite the presumed random configuration of the polymer, facetted growth faces are present, with the common orientation over the entire figure suggesting it is all part of one single crystal.

These observations of the terpolymers raise several questions. One would expect that if the chains are extended in the mesomorphic state, as is anticipated in all theories and models we know of (hairpins have been proposed [73] and reported based on small angle neutron scattering experiments (with a (tight) fold period of 200–300 Å) [74] but, from theory, are said to be few in number and decrease with decreasing temperature [75]), then the primary nuclei would also be chain extended rather than folded. *One thus has to conclude that either: (1) the chains are already folded in the nematic state* (Watanabe and co-workers, based on SAXS and TEM measurements of lamellar thicknesses of 250–480 Å in bulk samples of bi-benzoate-flexible segment LC co-polyesters, have made similar suggestions more recently [76–78]), *(2) the kinetic theories of crystallization do not apply, or (3) the surface is exerting an as yet unexplained influence.* One could suggest a combination of the first and third explanations; that the chains are folded in the thin films and near the surfaces in the mesomorphic state. However, this would not explain Watanabe's results or our observations of thinner, chain extended lamellae in quenched terpolyester. *We have thus gone full circle back to the initial question of the form of the primary nucleus for polymer single crystals, with the added questions, here, of the conformation in the mesomorphic state and the role of a surface in affecting the morphology of polymers crystallized in its presence.*

4. Summary

Most, but not all, polymer morphology research, both experimental and theoretical, has been directed at understanding the crystallization of polyethylene, most recently in its various forms with polypropylene probably being the next most studied. We suggest that the theories that are developed should be applicable to readily crystallizable polymers in general. Furthermore, we suggest that there are a number of observations, some described above, that date back to the beginnings, by Keller, Till, and Fischer [1–3], of modern polymer morphology investigations, that have been overlooked. We also suggest that, for some studies, polymers other than LPE and PP may be more suitable for developing appropriate models. For instance. POM is better for SAXS than LPE because of the minimal "void" scatter near the main beam, for spherulite growth mechanisms due to the possibility of growing hedrites as representative of "perfect" spherulites and for TEM since it is self-etching, degraded polymer removing itself from the sample surface.

In the above we have raised questions concerning: (1) the nature of the primary nuclei in solution and melt grown (from the mesomorphic state) single crystals; (2) the origin of the linear variation in apex angle and, apparently, fold plane orientation in BCMO single crystals; (3) the nature of the fold planes and mechanism of folding (possibility of precursors) in lath-like or ribbon crystals with irregular "fast" growth faces; (4) the presence, and origin of lamellar doubling, in PEO, POM and PTFE; (5) the relationship of the SAXS spacings $\mathscr{L}_1$ and $\mathscr{L}_2$ (also L_{c1}^{m} and L_{c2}^{m}) and the $\mathscr{L}_1/\mathscr{L}_2$ ratio to the lamellar thickness observed by TEM, and the effect of annealing thereon; (6) the effect of a free surface (and possibly a thin film) on the conformation of the molecule in the melt and the resultant morphology following crystallization; and (7) the possibility of significant chain folding in the mesomorphic state. All of these questions are ripe for further examination, particularly with the advent of the new scanning probe microscopies, but the choice of appropriate polymers will be paramount.

As indicated in Section 1, it is 44 years since I first saw an electron micrograph of a polyethylene single crystal and since Prof. Keller [2] proposed the concept of chain folding in his paper. It is also 39 years since I first prepared the monograph Polymer Single Crystals [54] for internal circulation at DuPont. It is both encouraging and discouraging that so many basic problems remain, encouraging in that there is still much interesting and, hopefully, practically useful research to do and discouraging when one considers the limited extent of our advance in the last 40 years in understanding polymer crystallization.

Acknowledgements

This research has been supported over the years by DuPont, ARO (Durham), PRF, the Camille Dreyfus Fund, Gore and Assoc. Inc., and, in particular, NSF (Polymers Program).

References

[1] Till P. J Polym Sci 1957;24:301.
[2] Keller A. Philos Mag 1957;2:1171.
[3] Fischer EW. Z Naturforsch 1957;12a:753.
[4] Hoffman JD, Lauritizen Jr. JI. J Res Natl Bur Stand, Sect A 1961;65:297.
[5] Hoffman JD, Miller RL. Polymer 1997;38:3151.
[6] Garber CA, Geil PH. Makromol Chem 1968;113:236.
[7] Geil PH. Polymer 1963;4:404.
[8] Blundell DJ, Keller A, Kovacs A. J Polym Sci B 1966;4:25.
[9] Garber CA, Geil PH. Kolloid Z Z Polym 1969;229:140.
[10] Rybnikar F, Yuan B-L, Geil PH. Polymer 1994;35:1831.
[11] Rybnikar F, Liu J, Geil PH. Macromol Chem Phys 1994;195:81.
[12] Rybnikar F, Liu J, Meyers A, Geil PH. Korean Polym J 1998;6:53–75.
[13] Rybnikar F, Geil PH. J Polym Sci, Polym Phys B 1997;35:1807.
[14] Lucero A, Rybnikar F, Long T-C, Liu J, Geil PH, Wall B, Koenig JL. Polymer 1997;38:4387.
[15] Liu J, Cheng SZD, Geil PH. Polymer 1996;37:1413.
[16] Liu J, Geil PH, Huh S-M, Jin J-I. Acta Polym 1996;47:290.
[17] Liu J, Geil PH, Huh S-M, Jin J-I. Polymer 1996;37:2205.
[18] Liu J, Rybnikar F, Geil PH. J Macromol Sci, Phys B 1996;35:375.

[19] Rybnikar F, Liu J, East AJ, Geil PH. J Polym Sci, Polym Phys Ed 1993;31:1923.
[20] Liu J, Sidoti G, Myers JA, Geil PH, Kim JC, Cakmak M. J Macromol Sci Phys B 1998;37:567.
[21] Liu J, Geil PH. J Macromol Sci Phys B 1997;36:263.
[22] Liu J, Geil PH. J Macromol Sci Phys B 1997;36:61.
[23] Liu J, Geil PH. J Polym Sci, Polym Phys B 1997;35:1575.
[24] Liu J, Long T-C, Geil PH, Rybnikar F. J Polym Sci, Polym Phys B 1996;34:2843.
[25] Heber I. Kolloid Z Z Polym 1964;194:7.
[26] Heber I, Lehman J. Kolloid Z Z Polym 1964;200:7.
[27] Morrow DR, Sauer J, Woodward AE. J Polym Sci C 1968;16:3401.
[28] Holland VF, Mitchell SB, Hunter WL, Lindenmeyer PH. J Polym Sci 1962;62:145.
[29] Klement J, Geil PH. J Polym Sci, Part A-2 1968;6:1381.
[30] Geil PH. J Polym Sci 1960;44:449.
[31] Holland VF. Makromol Chem 1964;71:204.
[32] Sakaoku K, Iwashima H, Miyanoki M, Nagamo U. Rep Prog Polym Phys, Jpn 1965;8:87.
[33] Barenberg SA. MS thesis, Case Western Reserve University, 1971.
[34] Kojima M. J Polym Sci, Part 2 1967;5:597.
[35] Alper R, Lundgren DA, Marchessault RH, Cote WA. Biopolymers 1964;1:545.
[36] Yokouchi M, Chatani Y, Tadakoro H, Teranishi K, Tani H. Polymer 1973;14:267.
[37] Birley C, Briddon J, Sykes KE, Barker PA, Organ SJ, Barham PJ. J Mater Sci 1995;30:633.
[38] Kyu T, Mehta R, Chiu H-W. Submitted for publication.
[39] Reneker DH, Geil PH. J Appl Phys 1960;31:1916.
[40] Barnes WJ, Price FP. Polymer 1964;5:283.
[41] O'Leary K, Geil PH. J Macromol Sci, Phys B 1967;1:147.
[42] Siegmann A, Geil PH. J Macromol Sci, Phys B 1970;1:557.
[43] Burmester A, Geil PH. In: Pae RD, Morrow DR, Chen Y, editors. Advances in polymer science and engineering, New York: Plenum Press, 1972. p. 42–100.
[44] Debye P, Anderson Jr. HR, Brumberger H. J Appl Phys 1957;28:679.
[45] Hsiao BS, Verma RK. J Synchrotron Rad 1998;5:23.
[46] Crist B. J Macromol Sci Phys 2000;B39:493.
[47] Bassett DC. Principles of polymer morphology. Cambridge: Cambridge University Press, 1981 (sect. 4.5.3).
[48] Yeh F, Hsiao BS, Chu B, Sauer BB, Flexman EA. J Polym Sci, Polym Phys 1999;37:3115.
[49] Reinhold Chr, Fischer EW, Peterlin A. J Appl Phys 1964;35:71.
[50] Crist B. J Polym Sci, Polym Phys Ed 1973;11:635.
[51] Geil PH. J Polym Sci, Part C 1966;13:149.
[52] Geil PH. Polymer single crystals. New York: Wiley/Interscience, 1963 (chap. 4).
[53] Hendus H. Ergeb Exact Naturwiss 1959;31:331.
[54] Brown RG, Eby RK. J Appl Phys 1964;35:1156.
[55] Fischer EW. Kolloid Z Z Polym 1969;231:458.
[56] Fischer EW. Kolloid Z Z Polym 1967;218:97.
[57] Goddar H, Schmidt GF, Fischer EW. Makromol Chem 1969;127:286.
[58] Statton WO, Geil PH. J Appl Polym Sci 1960;3:357.
[59] McCrum NG. J Polym Sci 1961;54:561.
[60] Takayanagi M, Minima S. Rep Prog Polym Phys Jpn 1964;7:241.
[61] Hosemann R, Bagchi SN. Direct analysis of diffraction by matter. Amsterdam: North-Holland, 1962.
[62] Siegmann A, Geil PH. Unpublished micrographs.
[63] Hsaio BS, Gardner KH, Wu DQ, Chu B. Polymer 1993;34:3986–96.
[64] Bunn CW, Cobbold AJ, Palmer RP. J Polym Sci 1958;28:365.
[65] Speerschneider CJ, Li CH. J Appl Phys 1962;33:1871.
[66] Geil PH, Anderson FR, Wunderlich B, Arakawa T. J Polym Sci A 1964;2:3707.
[67] Melillo L, Wunderlich B. Kolloid Z Z Polym 1972;250:417.
[68] Symons NKJ. J Polym Sci 1963;1:2843.
[69] Xu P, Yang J, Geil PH. Presented at Am. Phys. Soc. Meeting, March, 1999, New Orleans (submitted for publication).
[70] Bassett DC, Block S, Pirmarini GJ. J Appl Phys 1974;45:4146.
[71] Kent SL, Rybnikar F, Geil PH, Carter JD. Polymer 1994;35:1869.
[72] Kent SL, Geil PH. J Polym Sci, Polym Phys B 1992;30:1489.
[73] deGennes PG. In: Ciferri A, Krigbaum WR, Meyer RB, editors. Polymer liquid crystals, New York: Academic Press, 1982.
[74] Li MH, Brulet A, Keller P, Cotton JP. Neutron News 1997;8(2):16 (and references therein).
[75] Croxton CA. Macromolecules 1990;23:2270.
[76] Tokita M, Osada K, Yamada M, Watanabe J. Macromolecules 1998;31:8590.
[77] Tokita M, Takahashi T, Hayashi M, Inomata K, Watanabe J. Macromolecules 1996;29:1345.
[78] Tokita M, Osada K, Watanabe J. J Liq Cryst 1997;23:453.